6-8-2022

Preclinical and clinical evaluation of the LRRK2 inhibitor DNL201 for Parkinson's disease

Danna Jennings

Sarah Huntwork-Rodriguez

Anastasia G. Henry

Jennifer C. Sasaki

René Meisner

See next page for additional authors

Authors

Danna Jennings, Sarah Huntwork-Rodriguez, Anastasia G. Henry, Jennifer C. Sasaki, René Meisner, Dolores Diaz, Hilda Solanoy, Xiang Wang, Elvira Negrou, Vitaliy V. Bondar, Rajarshi Ghosh, Michael T. Maloney, Nicholas E. Propson, Yuda Zhu, Romeo D. Maciuca, Laura Harris, Angela Kay, Peter A. LeWitt, T. Alex King, Drew Kern, Aaron Ellenbogen, Ira Goodman, Andrew Siderowf, Jason Aldred, Omid Omidvar, Shababa T. Masoud, Sonnet S. Davis, Annie Arguello, Anthony A. Estrada, Javier de Vicente, Zachary K Sweeney, Giuseppe Astarita, Marie T. Borin, Bradley K. Wong, Harvey Wong, Hoang Nguyen, Kimberly Scearce-Levie, Carole Ho, and Matthew D. Troyer

PARKINSON'S DISEASE

Preclinical and clinical evaluation of the LRRK2 inhibitor DNL201 for Parkinson's disease

Danna Jennings[1]*†, Sarah Huntwork-Rodriguez[1]†, Anastasia G. Henry[1]†, Jennifer C. Sasaki[1], René Meisner[1], Dolores Diaz[1], Hilda Solanoy[1], Xiang Wang[1], Elvira Negrou[1]‡, Vitaliy V. Bondar[2], Rajarshi Ghosh[1], Michael T. Maloney[1], Nicholas E. Propson[1], Yuda Zhu[1], Romeo D. Maciuca[1], Laura Harris[1], Angela Kay[1], Peter LeWitt[3], T. Alex King[4], Drew Kern[5], Aaron Ellenbogen[6], Ira Goodman[7], Andrew Siderowf[8], Jason Aldred[9], Omid Omidvar[10], Shababa T. Masoud[1], Sonnet S. Davis[1], Annie Arguello[1], Anthony A. Estrada[1], Javier de Vicente[1], Zachary K. Sweeney[11], Giuseppe Astarita[12,13]§, Marie T. Borin[1], Bradley K. Wong[1], Harvey Wong[14], Hoang Nguyen[1], Kimberly Scearce-Levie[1], Carole Ho[1], Matthew D. Troyer[1]

Mutations in leucine-rich repeat kinase 2 (*LRRK2*) are the most common genetic risk factors for Parkinson's disease (PD). Increased LRRK2 kinase activity is thought to impair lysosomal function and may contribute to the pathogenesis of PD. Thus, inhibition of LRRK2 is a potential disease-modifying therapeutic strategy for PD. DNL201 is an investigational, first-in-class, CNS-penetrant, selective, ATP-competitive, small-molecule LRRK2 kinase inhibitor. In preclinical models, DNL201 inhibited LRRK2 kinase activity as evidenced by reduced phosphorylation of both LRRK2 at serine-935 (pS935) and Rab10 at threonine-73 (pT73), a direct substrate of LRRK2. Inhibition of LRRK2 by DNL201 demonstrated improved lysosomal function in cellular models of disease, including primary mouse astrocytes and fibroblasts from patients with Gaucher disease. Chronic administration of DNL201 to cynomolgus macaques at pharmacologically relevant doses was not associated with adverse findings. In phase 1 and phase 1b clinical trials in 122 healthy volunteers and in 28 patients with PD, respectively, DNL201 at single and multiple doses inhibited LRRK2 and was well tolerated at doses demonstrating LRRK2 pathway engagement and alteration of downstream lysosomal biomarkers. Robust cerebrospinal fluid penetration of DNL201 was observed in both healthy volunteers and patients with PD. These data support the hypothesis that LRRK2 inhibition has the potential to correct lysosomal dysfunction in patients with PD at doses that are generally safe and well tolerated, warranting further clinical development of LRRK2 inhibitors as a therapeutic modality for PD.

INTRODUCTION

Parkinson's disease (PD) is the second most common neurodegenerative disease, affecting about 1 to 2% of individuals aged 65 years or older, with a prevalence projected to increase substantially as the global population ages (*1*). Over the many years that patients with PD live with the disease, disabling motor and nonmotor symptoms emerge (*2*). Whereas current therapies can temporarily improve motor symptoms and provide some benefit for nonmotor symptoms, a major unmet need remains to identify disease-modifying treatments to reduce the progression of PD.

Variants in leucine-rich repeat kinase 2 (*LRRK2*) are one of the most common genetic risk factors in PD. *LRRK2*^{G2019S}, the most common pathogenic variant in *LRRK2*, accounts for a high proportion (about 4 to 5%) of familial PD cases and about 1% of sporadic PD cases (*3*). In addition, genome-wide association studies have shown that common noncoding variants at the *LRRK2* locus confer risk for PD (*4*). Several PD-associated *LRRK2* variants increase LRRK2 kinase activity, resulting in excessive phosphorylation of substrates. These substrates include a subset of Rab guanosine triphosphates (GTPases) that act as master regulators of intracellular trafficking (*5*). As LRRK2 variants increase the phosphorylation of several Rab GTPases and can affect their ability to interact with downstream effectors, LRRK2 kinase activity has been shown to play a role in regulating many aspects of membrane trafficking, including autophagy, retrograde transport from endosomes to the trans-Golgi network, and lysosomal function (*6*). In particular, LRRK2 activity can affect various aspects of endolysosomal function, including autophagic flux, protein degradation, and response to lysosomal damage (*7*).

Inhibition of LRRK2 activity and the consequent improvement of membrane trafficking and lysosomal function is a promising new approach for disease modification in PD (*7*). In addition to patients with PD who have *LRRK2* variants, increased LRRK2 activity has also been observed in patients with other genetic forms of PD (e.g., the D620N mutation in VPS35) and with nonhereditary idiopathic PD (*8*–*10*). Furthermore, increasing evidence from human genetic studies and preclinical PD animal models emphasizes that lysosomal dysfunction is a common hallmark of PD and suggests that therapeutic approaches aimed at improving PD-linked defects in lysosomal homeostasis, including LRRK2 inhibition, may meaningfully affect disease progression (*11*). For example, variants in the *GBA* gene, which encodes the lysosomal enzyme glucocerebrosidase

[1]Denali Therapeutics Inc., South San Francisco, CA, USA. [2]REGENXBIO, Rockville, MD, USA. [3]Henry Ford Health System, Detroit, MI, USA. [4]Covance, Dallas, TX, USA. [5]University of Colorado, School of Medicine, Aurora, CO, USA. [6]Michigan Institute for Neurological Disorders, Farmington Hills, MI, USA. [7]Bioclinica Research, Orlando, FL, USA. [8]University of Pennsylvania, Penn Neurology Pennsylvania Hospital, Philadelphia, PA, USA. [9]Inland Northwest Research, Spokane, WA, USA. [10]Collaborative Neuroscience Research, Long Beach, CA, USA. [11]Interline Therapeutics, South San Francisco, CA, USA. [12]Arkuda Therapeutics, Watertown, MA 02472, USA. [13]Biochemistry and Molecular & Cellular Biology, Georgetown University, Washington, DC 20057-1468, USA. [14]University of British Columbia, Vancouver, BC, Canada.
*Corresponding author. Email: jennings@dnli.com
†These authors contributed equally to this work.
‡Janssen Pharmaceuticals, South San Francisco, CA, USA.
§Present address: Biochemistry and Molecular and Cellular Biology, Georgetown University, Washington, DC, USA.

(GCase), are associated with the lysosomal storage disorder Gaucher disease and with increased risk for developing PD. Emerging data suggest that LRRK2 inhibition may lead to increased GCase activity and correct lysosomal deficits in cellular models carrying *GBA* variants, suggesting that LRRK2 inhibition may ameliorate lysosomal dysfunction more broadly than that caused by variants in *LRRK2* itself (*12*, *13*).

Markers of LRRK2 activity, such as posttranslational modifications of the protein itself and phosphorylation of downstream Rab substrates, can serve as tools to indicate the potency of LRRK2 inhibitors. The search for LRRK2 biomarkers in patients with PD has been extensive but relatively unsuccessful to date. An LRRK2 autophosphorylation site on serine-1292 can be quantified in exogenous expression systems, and there is evidence that amounts of both pS1292 LRRK2 and pT73 Rab10 in exosomes isolated from urine reflect LRRK2 activity (*14*, *15*). However, these techniques are not easily translatable to quantification of LRRK2 inhibition in human clinical samples such as urine, cerebrospinal fluid (CSF), blood, or blood-derived cells, e.g., peripheral blood mononuclear cells (PBMCs) (*16*).

Lysobisphosphatidic acid, also called BMP [bis(monoacylglycerol) phosphate], is an atypical, bioactive phospholipid that promotes lipid sorting in late endosomes and lysosomes. BMP plays a key role in regulating the activity of lysosomal hydrolases and serves as a biomarker of LRRK2-mediated effects on the lysosome. BMP is largely localized within the membranes of intralumenal vesicles of late endosomes and lysosomes. Changes in BMP concentration reflect functional changes in the lysosomal pathway and have been used to monitor lysosomal function in patients with lysosomal storage disorders, e.g., elevated BMP in the urine of patients with Niemann-Pick disease type C (*17*, *18*). Human *LRRK2*^{G2019S} carriers have higher concentrations of urine BMP compared with noncarriers (*19*). When LRRK2 activity is absent or reduced, as in *LRRK2* knockout mice or nonhuman primates treated with LRRK2 inhibitors, urine BMP concentrations are decreased (*20*). Thus, urinary BMP may be a useful marker to assess modulation of lysosomal function during treatment with LRRK2 inhibitors.

DNL201, referred to as GNE-0877 in previous publications (*21*, *22*), was developed for the treatment of PD. DNL201 is a first-in-class, selective, ATP (adenosine triphosphate)–competitive, orally bioavailable, central nervous system (CNS)–penetrant, small-molecule LRRK2 inhibitor. Compound 1 (Fig. 1A) was first reported in 2012 as a screening hit from a biochemical LRRK2 high-throughput screening assay (*23*). Through structure-based drug design using a

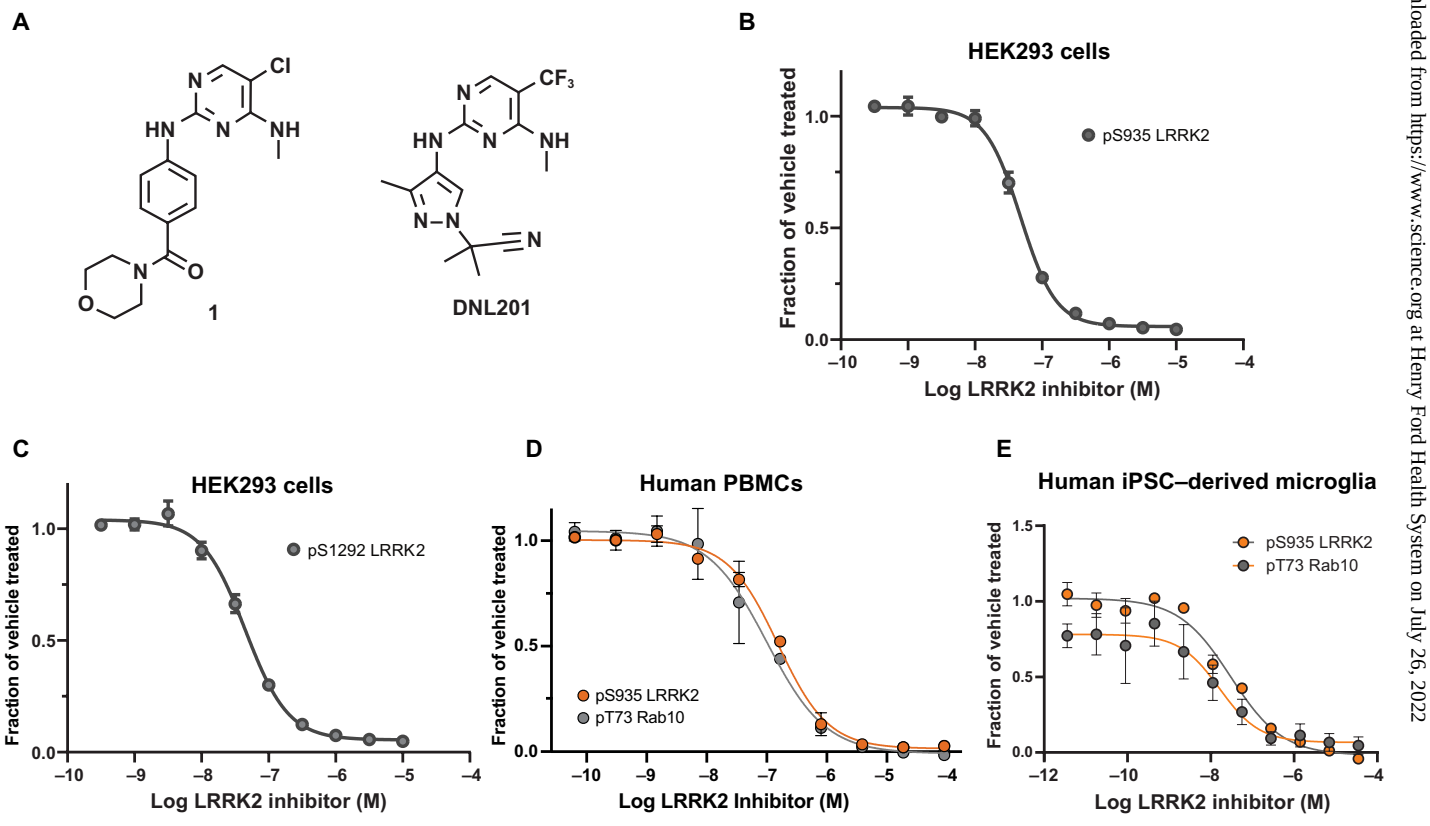

Fig. 1. Structure and potency of the LRRK2 inhibitor DNL201. (**A**) Structural comparison of biochemical high-throughput screen hit (compound 1) and DNL201. DNL201 is referred to as GNE-0877 in previous publications (*21*). (**B** and **C**) Dose-response curves of LRRK2 inhibition by DNL201 as measured by reduction of (B) pS935 and (C) pS1292 in HEK293 cells overexpressing LRRK2^{G2019S}. Dots and error bars indicate mean and SD of data points from two technical replicates in one experiment. IC_{50} values are geometric means, and ranges represent 95% confidence intervals (CIs): (B) pS935 IC_{50}, 47 nM (43 to 52 nM); (C) pS1292 IC_{50}, 45 nM (39 to 51 nM). (**D**) Ex vivo treatment of healthy human PBMCs with DNL201 decreased both pS935 LRRK2 and pT73 Rab10 in a dose-dependent manner ($n = 2$ donors) in one experiment. Dots and error bars indicate mean and SD of the two donors. IC_{50} values are geometric means, and ranges represent 95% CIs. pS935 IC_{50}, 53 nM (43 to 66 nM); pT73 Rab10 IC_{50}, 35 nM (22 to 56 nM). (**E**) Ex vivo treatment of human iMG with DNL201 treatment decreased both pS935 LRRK2 and pT73 Rab10 in a dose-dependent manner. Data are shown as means ± SEM; $n = 3$ independent experiments. IC_{50} values are geometric means, and ranges represent 95% CIs: pS935 IC_{50}, 30 nM (17 to 53 nM); pT73 Rab10 IC_{50}, 16 nM (0.4 to 86 nM).

validated LRRK2 homology model and CNS-focused medicinal chemistry optimization, Estrada *et al.* discovered aminopyrazole DNL201 [2-methyl-2-(3-methyl-4-((4-(methylamino)-5-(trifluoromethyl)pyrimidin-2-yl)amino)-1H-pyrazol-1-yl) propanenitrile, GNE-0877] (*21*). Off-target kinase profiling showed that DNL201 is a highly specific LRRK2 inhibitor with an acceptable in vitro biochemical selectivity window against off-target kinases. In vitro metabolism profiling of DNL201 revealed low turnover in human microsomes, and permeability assessment demonstrated that DNL201 is not a P-glycoprotein [MDCK-MDR1 (Madin-Darby canine kidney cells transfected with the human multidrug resistance 1 gene)] or breast cancer resistance protein (BCRP) transporter substrate (*21*). In vivo systemic pharmacokinetics assessment in preclinical species (mouse, rat, and cynomolgus macaque) demonstrated low clearance, moderate half-lives, and good oral bioavailability (*21*). In vivo CNS pharmacokinetic experiments across preclinical species confirmed that ratios of unbound brain and CSF concentrations of DNL201 to unbound plasma concentrations of DNL201 are near unity, confirming good penetration of DNL201 into the CNS. In animal models, LRRK2 inhibition has been associated with microscopic lung and renal changes, which were demonstrated to be nonadverse and reversible (*20*, *22*). Here, we present preclinical and clinical studies of DNL201, including safety, pharmacokinetics, and pharmacodynamics of DNL201 in healthy volunteers and in patients with PD.

RESULTS

DNL201 reduces LRRK2 activity and restores lysosomal function in cellular and animal models

The cellular potency of DNL201, whose structure is shown in Fig. 1A (*21*), was assessed in human embryonic kidney (HEK) 293 cells overexpressing LRRK2^{G2019S} using S935 and S1292 LRRK2 phosphorylation as measures of kinase activity (Fig. 1, B and C). The potencies for DNL201 using these two LRRK2 phosphorylation sites were equivalent, with a half-maximal inhibitory concentration (IC_{50}) in HEK293 cells of 47nM for pS935 LRRK2 and 45nM for pS1292. Using pS935 LRRK2 and pT73 Rab10 as readouts of LRRK2 inhibition, comparable potencies were measured in human PBMCs expressing wild-type LRRK2 (IC_{50} of 53 and 35 nM, respectively) (Fig. 1D). DNL201 treatment also led to a dose-dependent decrease in pS935 LRRK2 and pT73 Rab10 (IC_{50} of 30 and 16 nM, respectively) in human-induced pluripotent stem cell (iPSC)–derived microglia (iMG), confirming that similar inhibition was observed in relevant human CNS cells (Fig. 1E). To measure the potency of DNL201 in human cells expressing LRRK2^{G2019S}, human PBMCs from LRRK2^{G2019S} carriers and controls were analyzed ex vivo. Treatment with DNL201 effectively inhibited LRRK2 phosphorylation, with about twofold increase in potency of DNL201 in PBMCs from LRRK2^{G2019S} carriers versus controls (mean IC_{50}, 22 versus 50 nM) (fig. S1A). Increased potency of DNL201 was also observed in primary cortical neurons from LRRK2^{G2019S} knockin mice compared to wild-type controls (fig. S1B).

Next, the ability of DNL201 to rescue lysosomal defects in cellular models of disease was evaluated. Consistent with previous findings, overexpression of fluorescently tagged LRRK2^{G2019S} in human H4 neuroglioma cells led to enlarged lysosomes that coalesced and showed a perinuclear distribution (Fig. 2A) (*24*). DNL201 treatment restored lysosome size and morphology to that observed in cells expressing wild-type LRRK2 (Fig. 2A). To assess the effects of DNL201 on lysosomal function, the extent of lysosomal protein degradation was measured in wild-type and *LRRK2*^{G2019S} cells using a cellular model with endogenous expression of LRRK2^{G2019S}, that is, primary mouse astrocytes derived from *LRRK2*^{G2019S} knockin mice. Primary astrocytes from *LRRK2*^{G2019S} knockin mice showed a reduction in lysosomal protein degradation compared with cells derived from wild-type mice. After DNL201 treatment, lysosomal protein degradation was normalized back to wild-type levels in the *LRRK2*^{G2019S} primary mouse astrocytes (Fig. 2B; $P < 0.05$ and $P < 0.01$).

LRRK2 inhibition may also correct disease-associated lysosomal dysfunction independent of *LRRK2* mutation status. Patients who have homozygous loss-of-function mutations in the gene GBA can develop the lysosomal storage disorder Gaucher disease, and patients who have heterozygous *GBA* mutations have an increased risk for PD (*25*). Furthermore, recent findings in astrocytes from *GBA*^{D409V} knockin mice and iPSC-derived dopaminergic neurons from *GBA* variant carriers have shown that LRRK2 inhibition can boost GCase activity and correct downstream defects, suggesting that LRRK2 inhibition may be beneficial in normalizing lysosomal dysfunction caused by *GBA* variants (*12*, *13*, *26*). To assess the ability of LRRK2 inhibition to correct lysosomal dysfunction more broadly, fibroblasts from patients with Gaucher disease were treated with DNL201 (Fig. 2C). Treatment with DNL201 partially corrected dysfunctional lysosomal protein turnover in this aggressive cellular model of *GBA*-linked lysosomal dysfunction, suggesting that DNL201 treatment may correct lysosomal dysfunction not directly caused by variants in LRRK2 (Fig. 2C; $P < 0.01$).

DNL201 inhibits LRRK2 activity both in the periphery and CNS in animal models

The potency of DNL201 was assessed in the kidney and brain tissue of rats 1 hour after oral administration of DNL201 at 3, 10, 30, or 60 mg/kg. DNL201 inhibited pS935 LRRK2 in a dose-dependent manner in both kidney and brain tissue compared with vehicle-treated animals 1 hour after a single dose (Fig. 3, A and B, and fig. S2). By comparing drug exposure and pS935 LRRK2 inhibition in rat brain, an unbound IC_{50} of 52 nM in brain was calculated.

In vivo pharmacology was also assessed in cynomolgus macaques. Briefly, DNL201 (0.5 mg/kg) was administered by intravenous bolus injection to macaques that had a surgically implanted catheter in the cisterna magna for sampling of CSF. The unbound DNL201 concentrations were similar in plasma and CSF, indicating that measurement of DNL201 in blood correlated with the concentration in brain tissue (Fig. 3C). To assess the pharmacodynamic effects of DNL201 in the periphery and the CNS, PBMCs and brain tissues were collected from cynomolgus macaques treated with DNL201 for 28 days and euthanized 24 hours after the last dose. DNL201 exhibited similar dose-dependent inhibition of LRRK2 activity in PBMCs and brain homogenates from the animals as measured by pS935 LRRK2 (Fig. 3D), demonstrating that CNS pharmacodynamic effects of DNL201 can be predicted using LRRK2 inhibition. A dose-dependent reduction in phosphorylation of Rab12, a direct substrate of LRRK2, was also observed in macaque kidney and brain tissue after DNL201 treatment (fig. S3).

LRRK2 activity regulates the amount of the lysosomal marker BMP in urine and kidney in animal models

As BMP concentrations are elevated in the urine of LRRK2^{G2019S} carriers, and LRRK2 inhibition can reduce urinary BMP in rodents and nonhuman primates (*19*, *20*), the effect of LRRK2 inhibition on

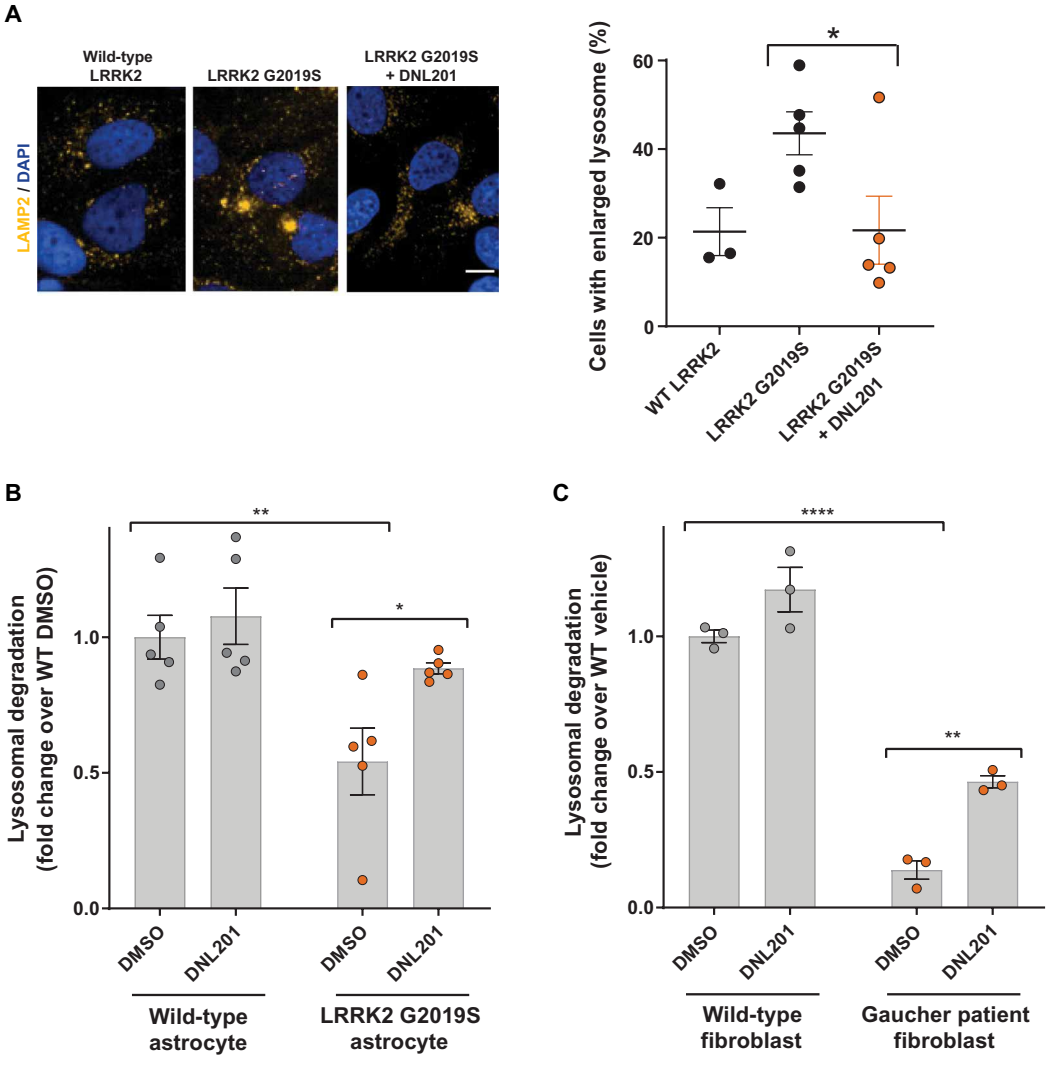

Fig. 2. DNL201 rescues lysosomal defects in cellular models. (**A**) H4 cells expressing wild-type LRRK2 or mutant LRRK2^{G2019S} were treated with vehicle or DNL201 (0.3 μM), fixed 72 hours after treatment, and stained using an antibody against LAMP1 to assess lysosome morphology. The percentage of cells with enlarged lysosomes was quantified. Data are shown as means ± SEM from three to five independent experiments *$P < 0.05$, unpaired *t* test. Scale bar, 10 μm. (**B**) Primary astrocytes from wild-type LRRK2 or mutant LRRK2^{G2019S} mice were treated with 2 μM DNL201 or DMSO vehicle control for 72 hours, and lysosomal protein degradation was assessed using an AHA-based assay. Data were normalized to the median within each experiment and then to the wild-type vehicle-treated group. Data are shown as means ± SEM; $n = 5$ independent experiments. *$P < 0.05$ and **$P < 0.01$, two-way ANOVA adjusted for multiple comparisons using Dunnett's method. (**C**) Lysosomal protein turnover in fibroblasts from healthy human controls and patients with Gaucher disease (*GBA* L444P variant carriers) after a 72-hour treatment with 2 μM DNL201 or DMSO vehicle control. Data were normalized to the median within each experiment and then to the healthy control, vehicle-treated group. Data are shown as means ± SEM; $n = 3$ independent experiments. **$P < 0.01$ ****$P < 0.0001$, two-way ANOVA adjusted for multiple comparisons using Dunnett's method.

BMP in kidney tissue of mice was evaluated to better understand how changes in urinary BMP relate to lysosomal function changes in the kidney. For this assessment, a tool LRRK2 inhibitor (MLi-2) was administered in the diet to wild-type and *LRRK2*^{G2019S} knockin mice for seven consecutive days, and the concentration of BMP in mouse urine and kidney was assessed to determine whether BMP changes in the kidney could account for LRRK2 activity–dependent changes in urine BMP. BMP concentrations were reduced in urine from both wild-type and *LRRK2*^{G2019S} knockin mice after MLi-2 treatment, which was consistent with previous reports (Fig. 3E) (*20*, *22*). In the renal cortex, genotype-dependent differences in BMP in the *LRRK2*^{G2019S} knockin mice were observed, showing significantly lower BMP concentrations compared with wild-type littermate controls (Fig. 3F; $P < 0.05$). After LRRK2 inhibition, kidney BMP concentrations were significantly increased in both wild-type and *LRRK2*^{G2019S} knockin mice (Fig. 3, F and G; $P < 0.05$, $P < 0.001$, and $P < 0.0001$). Whereas it may appear paradoxical that LRRK2 inhibition increased BMP in kidney while decreasing BMP in urine, this finding is consistent with data demonstrating that BMP can be an actively secreted lysosomal lipid (*27*). Together, these results suggest that LRRK2 inhibition may decrease the extracellular release of BMP-containing vesicles from kidney cells.

Safety of chronic DNL201 treatment in animals

Previously reported toxicology studies with LRRK2 inhibitors were short term and included ≤28 days of repeat dosing (*20*, *22*). In a

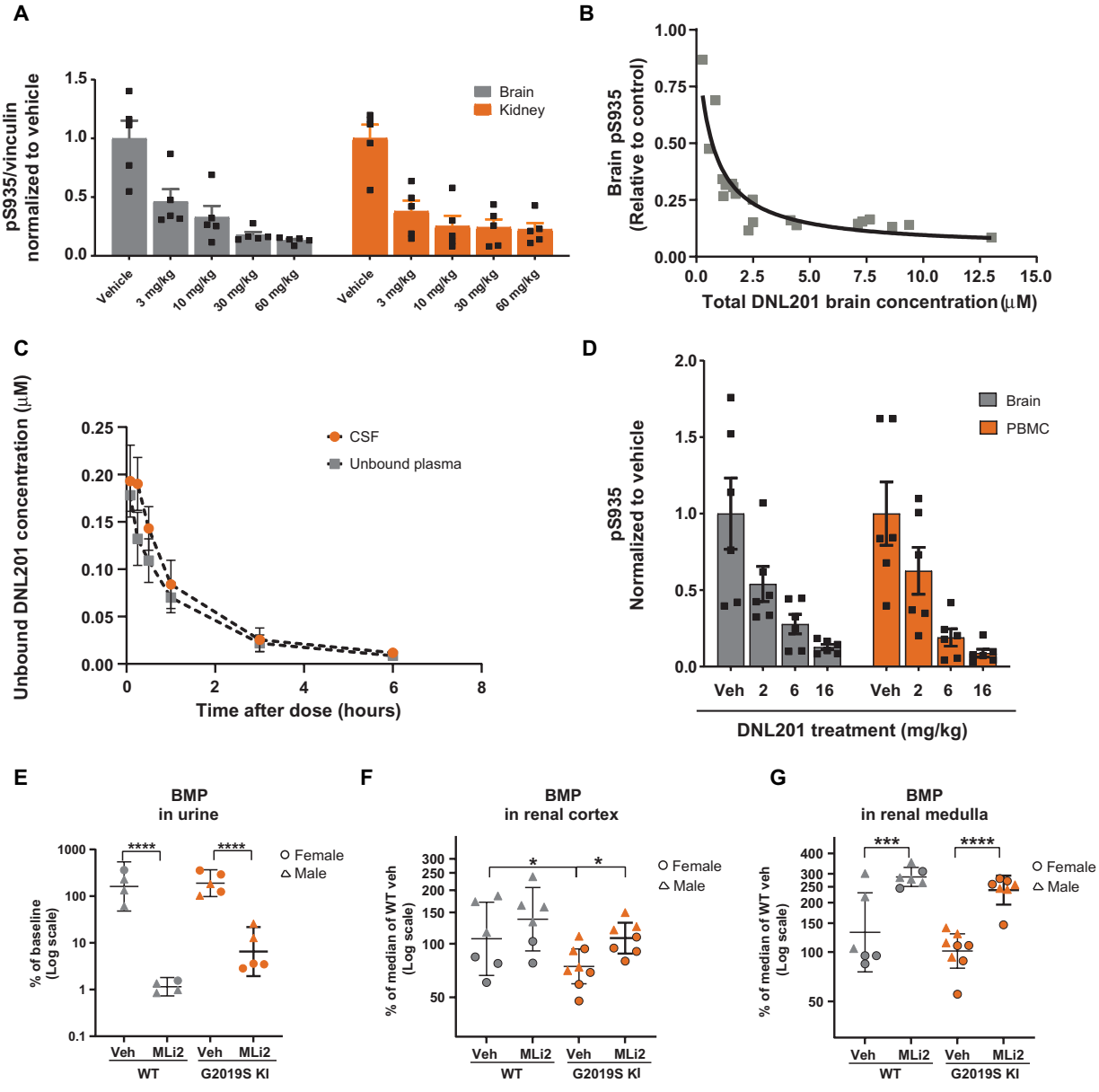

Fig. 3. DNL201 inhibits LRRK2 in the periphery and CNS of rodents and macaques. (**A**) DNL201 inhibited pS935 LRRK2 in a dose-dependent manner in both kidney and brain of treated rats compared to animals given vehicle. Amounts of pS935 LRRK2 and vinculin after treatment with increasing doses of DNL201 or vehicle were assessed by Western blot analysis. The amount of pS935 LRRK2 was normalized to vinculin to control for protein loading. Quantification for each condition was normalized to that for the vehicle-treated group. The bar graphs represent the means ± SEM. Black squares represent individual measured values for each animal ($n = 5$) in one experiment. (**B**) DNL201 inhibited pS935 LRRK2 in a concentration-dependent manner in rat brain. Plot of brain pS935 LRRK2 versus total DNL201 brain concentrations generated from data shown in (A). Gray squares represent individual measured values for each animal. Line represents inhibitory imax model fit. (**C**) Free (unbound) DNL201 concentrations over time in plasma and CSF of cynomolgus macaques. Unbound concentrations of DNL201 in plasma were calculated from total DNL201 concentrations in plasma by applying an unbound fraction of 0.21, which was determined using pooled macaque plasma by an equilibrium dialysis method. Plots show means ± SD of three animals. (**D**) LRRK2 inhibition by DNL201 in macaque brain and macaque PBMCs was measured by quantitating pS935 LRRK2. PBMCs and brain samples from cynomolgus macaques treated with DNL201 BID at the doses shown (2, 6, and 16 mg/kg) or vehicle (veh) for 28 days were collected 24 hours after the last dose (day 29). pS935 LRRK2 was quantified relative to the average pS935 LRRK2 measurement in the vehicle group. Plots show means ± SEM; $n = 6$ animals per dose group. No significant differences were found between pS935 LRRK2 relative to the vehicle group in the brain compared to PBMCs ($P > 0.5$ for group mean comparisons by dose in the brain versus PBMCs by *t* test). (**E** to **G**) *LRRK2*^{G2019S} knockin (KI) mice and wild-type (WT) littermates were administered a tool LRRK2 inhibitor (MLi-2) in chow, and concentrations of a specific species of BMP (22:6/22:6) were measured in urine and in the renal cortex and renal medulla 7 days after dosing using liquid chromatography tandem mass spectrometry. (E) Terminal BMP (22:6/22:6) concentrations (relative abundance) in urine were normalized as a percentage of predosed BMP concentrations ($n = 4$ to 5 mice). (F and G) BMP (22:6/22:6) concentrations were quantified in the renal cortex and renal medulla and normalized as a percent of median values from the WT vehicle group ($n = 6$ to 8 mice). Individual animal data are plotted (stratified by sex). Gray, WT mice; orange, *LRRK2*^{G2019S} KI mice. Data are shown as geometric means with 95% CIs. *$P < 0.05$, ***$P < 0.001$, ****$P < 0.0001$ based on an ANCOVA model derived based on an ANCOVA model with terms for treatment, genotype, treatment by genotype interaction, with adjustment for sex, and for urine, by predose BMP levels, with statistical significance assessed at nominal levels.

chronic toxicity study in macaques lasting 39 weeks, a duration considered suitable to detect late-occurring toxicities and progression of identified findings (*28*), DNL201 was tolerated up to the highest tested dose of 32 mg/kg per day (16 mg/kg twice daily or BID), with corresponding peak plasma concentration (C_{max}) and area under the plasma concentration-time curve [$AUC_{(0-24h)}$] values of 7.33 and 98.9 μM/hour, respectively (Table 1). No DNL201-related mortality occurred in this study. In addition, no treatment-related effects on vital signs were observed, including pulse oximetry and respiration rates (tables S1A and S1B).

DNL201 treatment was associated with microscopic lung changes in cynomolgus macaques consisting of vacuolated type II pneumocytes that were nonadverse and reversible (fig. S4 and table S2). The observed lung effects have been previously described and attributed to on-target LRRK2 kinase inhibition across multiple compounds (*20*, *22*). No increase in vacuolated type II pneumocytes was observed in the lungs of animals receiving 4 mg/kg BID DNL201, whereas minimal to slightly increased numbers were observed in the lungs of animals receiving 8 mg/kg BID or 16 mg/kg BID (orally) for 39 weeks (table S2). These changes were not associated with cellular injury or inflammation when evaluated by light or electron microscopy and did not increase in severity after 9 months of treatment compared with shorter studies (*20*, *22*). After a 12-week treatment-free period, type II pneumocyte vacuolation was fully reversible (table S2). The original 12-week and this 39-week study of DNL201 treatment effects revealed similar microscopic lung findings, with no observed clinical pulmonary dysfunction in nonhuman primates. Because of the lack of progression of the lung changes, clinical signs of pulmonary dysfunction, or secondary effects (e.g., lung cellular injury or inflammation) in nonhuman primates, DNL201 is not expected to affect respiratory function in humans at doses in the therapeutic range.

In the kidneys, reversible, nonadverse, minimally or slightly increased pigment was observed in renal tubular epithelial cells at >8 mg/kg BID of DNL201 in macaques after 39 weeks of treatment (table S2). These findings in the kidney are morphologically consistent with findings described in *LRRK2* knockout mice and rats (*29*, *30*). Clinical pathology evaluation of urinary function included clinical chemistry, urinalysis, and urine chemistry (table S3, A and B). No DNL201-related effects on renal function were observed.

LRRK2 activity is increased in patients with sporadic PD and in *LRRK2*^{G2019S} carriers relative to non-PD and noncarrier controls

To help define the level of inhibition needed to normalize LRRK2 kinase activity in patients with PD, the question of whether pT73 Rab10, an LRRK2 substrate that can be measured in PBMCs, could serve as a proximal marker of LRRK2 activity was investigated. PBMCs were isolated from *LRRK2*^{G2019S} mutation carriers (with and without PD), patients with sporadic PD, and healthy volunteers (controls) (table S4). As total LRRK2 in human PBMCs varies widely among individuals (*31*), the amount of pRab10 was normalized to total LRRK2 as a metric of LRRK2 activity. After normalizing to total LRRK2, pT73 Rab10 was elevated by about twofold in patients with sporadic PD and in *LRRK2*^{G2019S} mutation carriers compared to healthy volunteers (fig. S5), suggesting elevated LRRK2 activity in these populations.

Other groups have measured pT73 Rab10 or phosphorylation stoichiometry in neutrophils, a subset of cells in peripheral blood that express both LRRK2 and Rab10, in patients with sporadic PD and *LRRK2*^{G2019S} carriers with and without PD. Results from these studies vary from no detectable increase in pT73 Rab10 to about twofold increase in pT73 Rab10 in *LRRK2*^{G2019S} carriers versus noncarriers (*32*–*36*). The results of the present study are consistent with this range of modestly elevated pT73 Rab10 in *LRRK2*^{G2019S} carriers versus noncarriers, suggesting that ≤2-fold increase in LRRK2 kinase activity may be sufficient to confer an elevated lifetime risk of developing PD. Together with other published data on the degree of elevated Rab10 phosphorylation due to *LRRK2*^{G2019S} (*5*, *37*) and recent data showing an about twofold increase in LRRK2^{G2019S} kinase activity compared with wild-type LRRK2 based on an assay of intrinsic LRRK2 kinase activity (*38*), these data also suggest that 50% inhibition of LRRK2 kinase activity, at a minimum, may likely be needed in clinical studies to achieve therapeutic efficacy for slowing disease progression. Although *LRRK2*^{G2019S} is by far the most common pathogenic *LRRK2* variant in the Americas, Europe, and Northern Africa, most PD-associated LRRK2 variants have also been reported to increase kinase activity directly or indirectly (*39*). The degree of elevation of Rab10 phosphorylation in peripheral immune cells or other tissue samples derived from carriers of these additional PD-causing *LRRK2* variants beyond the *G2019S* mutation is not yet well defined. Preliminary data in cell lines, mouse tissues, and neutrophils from a limited number of *LRRK2*^{R1441G} carriers suggest that kinase activity for some point mutations is elevated by more than the twofold seen in *LRRK2*^{G2019S} carriers, supporting 50% or greater LRRK2 inhibition as a minimum target for therapeutic efficacy in clinical studies (*5*, *33*, *37*).

DNL201 inhibits LRRK2 activity and modulates lysosomal biomarkers in healthy human volunteers and in patients with PD

Having established the acceptable nonclinical profile of DNL201 in rodents and nonhuman primates, human testing of LRRK2 inhibition

Table 1. Toxicity and plasma concentrations of DNL201 in cynomolgus macaques after 39 weeks of treatment.

Duration of dosing (recovery period)	Dosing	Animals (recovery)	Lung histopathology	Observed mean plasma concentrations	
				C_{max} (μM)	AUC_{0-24} (μM/hour)
9 months (3 months)	2 mg/kg BID (8 mg kg^{-1} day^{-1})	3 (2)	None	0.971	11.0
	8 mg/kg BID (16 mg kg^{-1} day^{-1})	3 (2)	Minimal increased vacuolation, type II pneumocytes	3.09	36.2
	16 mg/kg BID (32 mg kg^{-1} day^{-1})	3 (2)	Minimal to slightly increased vacuolation, type II pneumocytes	7.33	98.9

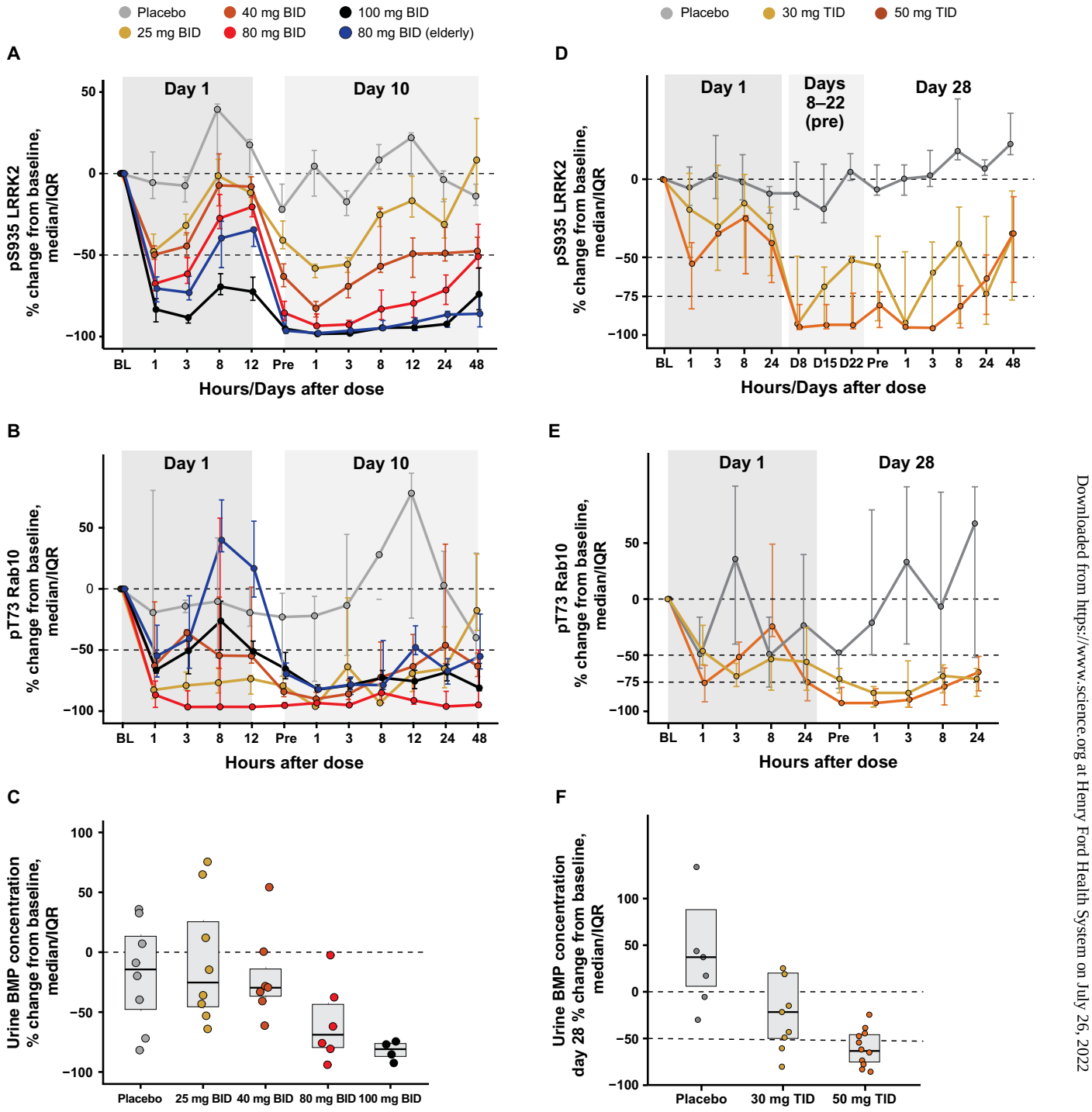

Fig. 4. Pharmacodynamics of LRRK2 inhibition. The pharmacodynamics of LRRK2 inhibition in healthy volunteers from the phase 1 study MAD cohorts (**A** to **C**) and in patients with PD in the phase 1b study (**D** to **F**) is shown. (A and D) pS935 LRRK2 reduction in whole blood in (A) healthy volunteers at days 1 and 10 after treatment with different doses of DNL201 and (D) in patients with PD at days 1, 8, 15, 22, and 28 after treatment with different doses of DNL201. (B and E) pT73 Rab10 reduction in PBMCs from (B) healthy volunteers at days 1 and 10 after treatment with different doses of DNL201 and (E) in patients with PD at days 1 and 28 after treatment with different doses of DNL201. (A to E) Pre, predose (sample collected just before the first dose on that day); BL, baseline (sample collected before the initiation of dosing). Data are expressed as median percent change from baseline. Error bars show interquartile ranges. (C and F) The reduction in urine BMP (22:6/22:6) normalized to urine creatinine from a baseline sample collected before the initiation of dosing in (C) healthy volunteers on the 10th day of treatment with different doses of DNL201 (postdose sample collected as a pooled sample 0 to 6 hours after the last dose) and (F) patients with PD on the 28th day of treatment with different doses of DNL201 (postdose sample collected as a pooled sample 1 to 6 hours after the last dose). Box plots show median percent change from baseline with interquartile ranges. (A) and (B) n=9-10 placebo, n=8 each DNL201 group; (C) BID dosing cohorts: n=8 Placebo, n=8 in 25 mg, n=7 in 40 mg, n=6 in 80 mg, n=4 in 100 mg. (D), (E) and (F) TID dosing cohorts: n=7 in placebo, n=9 in 30 mg, n=11 in 50 mg, n=6 in placebo, n=8 in 30 mg, n=11 in 50 mg.

was initiated. Safety, tolerability, pharmacodynamics, and pharmacokinetics of DNL201 were assessed in two human studies: (i) a phase 1, double-blind, placebo-controlled, first-in-human single ascending (SAD) and multiple ascending (MAD) dose study in healthy volunteers (NCT04551534) and (ii) a phase 1b, double-blind, placebo-controlled study enrolling patients with PD, both LRRK2 mutation carriers and noncarriers (NCT03710707).

In the phase 1 study, target and pathway engagement were evaluated by measuring pS935 LRRK2 in whole blood and pT73 Rab10 in PBMCs of 122 healthy volunteers (Fig. 4). In healthy volunteers receiving multiple doses of DNL201 for up to 28 days, a dose-dependent reduction from baseline was observed in pS935 LRRK2 and pT73 Rab10 (Fig. 4, A and B, and fig. S6). DNL201 exhibited strong LRRK2 inhibition, measured by whole-blood pS935 LRRK2, with 75 to 82% median reduction from baseline averaged over the 12-hour dosing interval on the final dosing day (day 10) at 80 and 100 mg BID. DNL201 treatment reduced urinary BMP concentrations (day 10) in healthy volunteers receiving 80 and 100 mg BID, consistent with modulation of lysosomal pathways (Fig. 4C).

LRRK2 target and lysosomal pathway engagement were also evaluated in the phase 1b study in 28 patients with mild to moderate PD. In patients with PD, a dose-dependent median reduction from baseline was observed in whole-blood pS935 LRRK2 averaged over the 12-hour dosing interval on the last dosing day (day 28) [>85% median reduction from baseline at 50 mg three times daily (TID) and > 55% median reduction from baseline at 30 mg TID] (Fig. 4D). In PBMCs from PD patients, pT73 Rab10 was also reduced by a median from baseline of >79 and ≥87% averaged over the 12-hour dosing interval on the last dosing day (day 28) in the 30- and 50-mg TID groups, respectively (Fig. 4E). This effect was associated with a reduction in urinary BMP concentration with the 50-mg TID dose (Fig. 4F). This suggested the potential for reversal of the lysosomal pathway defects that are present in LRRK2^{G2019S} mutation carriers who show elevated urinary BMP concentrations (*19*). Overall, the pharmacodynamic profile and the magnitude of inhibition of LRRK2 with DNL201 were similar among the healthy volunteers and patients with PD. However, the limited sample size of the LRRK2^{G2019S} carriers did not allow for a meaningful comparison of DNL201 potency among LRRK2^{G2019S} carriers, noncarriers with PD, and healthy volunteers.

DNL201 is safe and generally well tolerated in healthy volunteers and patients with PD

Safety and tolerability of DNL201 were assessed in the phase 1 SAD and MAD study in healthy volunteers. Sixty-three healthy volunteers were randomized in the SAD cohorts (age range, 18 to 50 years). Forty-seven received DNL201 at doses ranging from 10 to 225 mg, and 16 received placebo for 10 days; this group included 7 elderly healthy volunteers (mean age, 64.5 years), of whom 5 received 60 mg of the drug and 2 received placebo for 10 days. For the MAD cohorts, 59 healthy volunteers were randomized, with 48 receiving DNL201 at doses ranging from 40 mg once daily (QD) to 100 mg BID and 11 receiving placebo for 10 days; this group included 10 elderly healthy volunteers (8 receiving 80 mg BID DNL201 and 2 receiving placebo) (fig. S7A). The baseline characteristics of the healthy volunteers are presented in tables S5 and S6.

Table 2. Baseline demographics, clinical characteristics, and patient disposition for the phase 1b study.

Patient characteristics	Placebo (*n* = 7)	DNL201, 30 mg TID (*n* = 9)	DNL201, 50 mg TID (*n* = 12)	All patients (*n* = 28)
Demographics				
Age, median (range), years	66 (49–73)	62 (55–73)	57 (37–71)	63 (37–73)
Male sex, *n* (%)	5 (71)	8 (89)	9 (75)	22 (79)
LRRK2 PD mutation, *n* (%)	3 (43)	2 (22)	4 (33)	9 (32)
Baseline PD medications, *n* (%)				
MAO_B inhibitor (rasagiline or selegiline)*	1 (14)	4 (44)	6 (50)	11 (39)
Dopamine replacement	7 (100)	7 (78)	6 (50)	20 (71)
Dopamine agonist	2 (29)	3 (33)	5 (42)	10 (36)
None of the above	0	1 (11)	2 (17)	3 (11)
Disease status				
PD duration, median (range), years	3.4 (1–6)	3.3 (1–14)	3.6 (0–8)	3.4 (0–14)
Baseline MDS-UPDRS part III ("off" state) score, median (range)	29 (16–62)	29 (16–37)	29 (10–63)	29 (10–63)
Baseline MoCA score, median (range)	29 (26–30)	27 (25–30)	28.5 (26–30)	28 (25–30)
Disposition, *n* (%)				
Completed treatment	7 (100)	9 (100)	11 (92)	27 (96)
Discontinued study	0	0	1 (8)	1 (4)
Had blinded dose reduction	0	0	1 (8)	1 (4)

*One patient received selegiline, and 10 received rasagiline.

In the phase 1b study, DNL201 was investigated in a total of 28 patients with mild to moderate PD receiving standard-of-care therapy (fig. S7B), with values on the modified Hoehn and Yahr scale of 1 to 3. The PD patients were treated TID for 28 days with placebo (n = 7), DNL201 30 mg (n=9), or DNL201 50 mg (n = 12). Nine patients with PD (32%) had an LRRK2 coding variant: eight had the PD-associated G2019S mutation, and one had a rare LRRK2 variant of unknown significance (H365N). The baseline characteristics of the patients with PD are presented in Table 2.

In the phase 1 SAD and MAD cohorts of healthy volunteers, plasma DNL201 concentrations increased with increasing dose (Fig. 5, A and B, and tables S7 and S8). In the SAD cohorts, DNL201 exposure (AUC and C_{max}) increased in a slightly-greater-than-dose-proportional manner after single-dose oral administration over the 10- to 150-mg dose range. Median time to peak plasma concentration (t_{max}) for DNL201 was achieved at around 1 to 2 hours after dose under fasting conditions. In nonelderly healthy volunteers administered a single dose of DNL201 at 10 to 225 mg under fasting conditions, the mean ± SD terminal elimination half-life ranged from 7.5 ± 5.2 hours to 14.4 ± 4.4 hours (table S7). In elderly healthy volunteers receiving the 60-mg single dose, DNL201 exhibited a slightly longer mean ± SD terminal half-life of 17.4 ± 5.8 hours versus 12.9 ± 3.5 hours and a greater mean ± SD AUC from time zero to infinity ($AUC_{0-\infty}$) of 7.46 ± 2.62 μM*hour versus 4.51 ± 2.43 μM*hour compared to nonelderly healthy volunteers receiving the same dose. In the MAD cohorts, DNL201 exposure at steady state, the time after which the concentration of drug in the body remains consistent, as measured by steady-state AUC (AUC_{ss}) and steady-state C_{max} ($C_{max,ss}$) after BID multiple dosing, was overall slightly greater than dose proportional over the entire dose range evaluated (25 to 100 mg) (table S8). Steady state was achieved between days 8 and 10, as evidenced by similar mean AUC_{ss} and $C_{max,ss}$ values; mean accumulation ratios (AUC_{0-12h} on day 10/AUC_{0-12h} on day 1, and C_{max} on day 10/C_{max} on day 1, respectively) were about 1.2- to 2.3-fold for AUC_{0-12h} and about 1.0- to 1.7-fold for C_{max} in the nonelderly healthy volunteer BID MAD cohorts. After BID dosing at 80 mg for 10 days, the mean ± SD AUC_{ss} for DNL201 was greater in elderly healthy volunteers, 17.5 ± 7.5 μM*hour, than in nonelderly healthy volunteers, 11.8 ± 4.6 μM*hour, but with comparable mean ± SD terminal half-lives of 30.0 ± 9.7 hours versus 27.9 ± 16.3 hours, respectively. CSF–to–unbound plasma concentration ratio mean ± SD was 1.2 ± 0.15 and 0.87 ± 0.23 in nonelderly healthy volunteers receiving 25 and 80 mg BID, respectively, using an unbound fraction of DNL201 in human plasma of 25% (as determined from in vitro plasma protein binding using ultracentrifugation and equilibrium dialysis methods). The mean ± SD CSF–to–unbound plasma concentration ratio in elderly healthy volunteers receiving 80 mg BID was 1.0 ± 0.13 (fig. 5C). These CSF–to–unbound plasma ratios of DNL201, similar to what was observed in nonclinical species, suggest a high level of brain exposure for DNL201 in humans.

DNL201 was generally well tolerated in the phase 1 healthy volunteer study, at doses of ≤150 mg QD in the SAD cohorts and ≤100 mg BID in the MAD cohorts. No serious adverse events (SAEs) were observed. The most common treatment-emergent AEs (TEAEs) in the MAD cohorts that were more frequent in those who received DNL201 versus placebo were headache (40%), dizziness (13%), and nausea (13%). Across single and multiple doses, the nature and frequency of TEAEs were similar between the elderly and nonelderly healthy volunteer cohorts that received DNL201.

In the SAD cohorts, TEAEs were reported for 36% (17 of 47 volunteers) and 19% (3 of 16 volunteers) across all DNL201 dosing and placebo groups, respectively (table S9). All TEAEs were mild, with no discontinuations from study drug due to TEAEs. The most common TEAE in DNL201-treated healthy volunteers across all single-dose groups was headache (19%, 9 of 47 healthy volunteers). In the MAD cohorts, TEAEs were reported in 52% (25 of 48 healthy

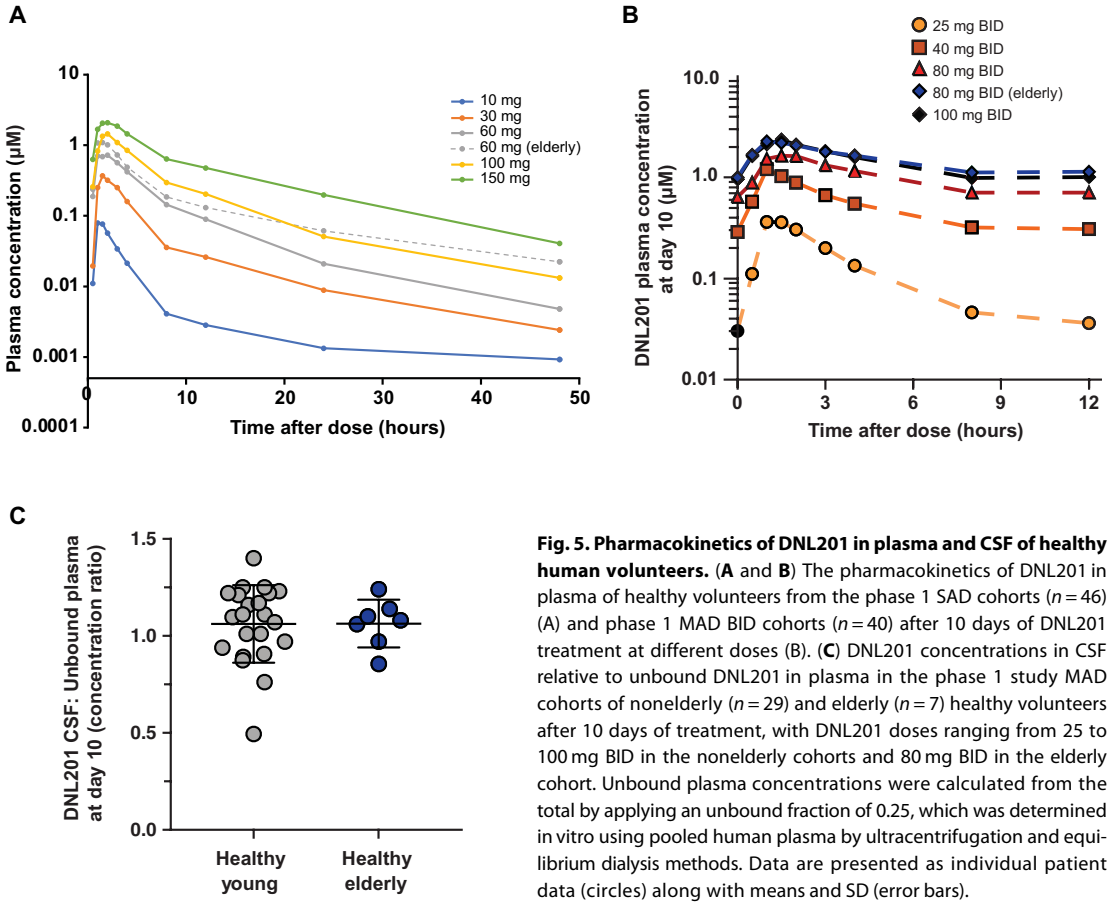

Fig. 5. Pharmacokinetics of DNL201 in plasma and CSF of healthy human volunteers. (**A** and **B**) The pharmacokinetics of DNL201 in plasma of healthy volunteers from the phase 1 SAD cohorts (n = 46) (A) and phase 1 MAD BID cohorts (n = 40) after 10 days of DNL201 treatment at different doses (B). (**C**) DNL201 concentrations in CSF relative to unbound DNL201 in plasma in the phase 1 study MAD cohorts of nonelderly (n = 29) and elderly (n = 7) healthy volunteers after 10 days of treatment, with DNL201 doses ranging from 25 to 100 mg BID in the nonelderly cohorts and 80 mg BID in the elderly cohort. Unbound plasma concentrations were calculated from the total by applying an unbound fraction of 0.25, which was determined in vitro using pooled human plasma by ultracentrifugation and equilibrium dialysis methods. Data are presented as individual patient data (circles) along with means and SD (error bars).

volunteers) and 55% (6 of 11 healthy volunteers) across all DNL201 dosing and placebo groups, respectively (table 3). Most TEAEs were mild in severity. TEAEs leading to study drug discontinuation were reported for three healthy volunteers (two with headache and one with atrial fibrillation considered unrelated to study drug), all of whom received DNL201. The most common TEAE in DNL201-treated healthy volunteers across all MAD cohorts was headache (40%, 19 of 48). Modest C_{max}-related increases in supine heart rate (about 10 bpm), as well as reductions in supine systolic blood pressure (about 5 to 10 mmHg), occurred at doses ≥100 mg BID and were generally asymptomatic. The hemodynamic changes were considered to be possibly related to off-target inhibition of phosphodiesterase $(PDE)_{3A}$ (IC_{50} of 0.73 μM) and PDE_5 (IC_{50} of 1.2 μM) by DNL201. The maximum tolerated dose for DNL201 was 100 mg BID as healthy volunteers initially given DNL201 at 150 mg BID required dose reduction to 100 mg BID on day 2 due to reports of mild dizziness (lightheadedness) in two participants and asymptomatic orthostatic hypotension in another participant.

To mitigate the modest C_{max}-related hemodynamic changes observed with BID doses ≥100 mg in the phase 1 study, TID dosing was implemented in the phase 1b study in patients with PD. After the first dose of DNL201 on day 1 (30 or 50 mg), the rate of absorption of DNL201 was similar for the two active treatment groups, with a median (range) for t_{max} of about 1.6 hours (1.0 to 3.0 hours) and 1.2 hours (0.97 to 3.0 hours), respectively. Mean C_{max} and AUC_{0-8h} of DNL201 increased in a greater-than-dose-proportional manner; mean increases in these parameters were about 2.7- and 2.0-fold, respectively, with an about 1.7-fold DNL201 dose increase from 30 to 50 mg. On day 28, the rate of absorption of DNL201 was similar for the two treatment groups, with a median (range) t_{max} of around 1.0 hour (0.5 to 8.0 hours) and 1.5 hours (1.0 to 4.0 hours), respectively (table S10). The mean terminal half-life was also similar for both treatment groups. The mean $C_{max,ss}$ and AUC_{ss} over the 8-hour dosing interval ($AUC_{0-8h,ss}$) of DNL201 increased in a greater-than-dose-proportional manner; mean increases in these parameters were about 1.9- and 2.3-fold, respectively, with an about 1.7-fold DNL201 dose increase from 30 to 50 mg TID. Clear separation in drug exposure was observed between the 30- and 50-mg doses (fig. S8A). The mean ± SD CSF–to–unbound plasma concentrations were about 1.1 ± 0.12 and 1.3 ± 0.25 for the DNL201 30- and 50-mg TID groups, respectively (fig. S8B).

In the phase 1b study, DNL201 was generally well tolerated in patients with PD at doses of 30 or 50 mg TID (Table 3). Most TEAEs were mild or moderate in severity in both DNL201 groups in the phase 1b study. A higher incidence of moderate TEAEs was seen in the 50-mg drug group (50 versus 0% in the placebo and 30-mg groups). The most common TEAE in the active-treatment groups was headache (7 of 21 patients, 33%). For both doses of DNL201, study drug–related TEAEs were generally manageable and reversible. The 30-mg group had one SAE of *Legionella* pneumonia, which began after completion of treatment and was reported as unrelated to study drug. One event of severe headache in a patient who received 50 mg TID led to a dose reduction; the headache resolved while the patient received 30 mg TID. One patient receiving 50 mg TID withdrew early from the study after experiencing moderate symptomatic orthostatic hypotension, moderate headache, and mild nausea. These events resolved without intervention upon discontinuation of study drug.

No clinically meaningful changes or dose-related trends in vital signs were observed with the exception of increased standing heart rate in two patients receiving 50 mg TID of DNL201. One patient had preexisting autonomic dysfunction, and one was receiving concomitant α-blocker (tamsulosin) treatment; both events were considered possibly related to DNL201. No clinically meaningful changes

Table 3. Common treatment-emergent adverse events in healthy volunteers in the phase 1 MAD cohorts and in the phase 1b PD cohort. For each TEAE, the number of participants experiencing ≥1 TEAE is shown, and if the participant experienced this TEAE on >1 occasion, it was counted once. TEAEs that occurred in ≥2 participants in any dosing group are also included.

	Phase 1 MAD healthy volunteer cohorts									Phase 1b PD cohort			
TEAE, *n* (%)	**PBO elderly (*n* = 2)**	**PBO (*n* = 9)**	**Total DNL201 (*n* = 48)**	**40 mg QD (*n* = 8)**	**25 mg BID (*n* = 8)**	**40 mg BID (*n* = 8)**	**80 mg BID (*n* = 8)**	**80 mg BID elderly (*n* = 8)**	**100 mg BID (*n* = 8)**	**PBO (*n* = 7)**	**Total DNL201 (*n* = 21)**	**30 mg TID (*n* = 9)**	**50 mg TID (*n* = 12)**
Participants with ≥ 1 TEAE, *n* (%)													
Any TEAE	1 (50)	5 (56)	25 (52)	3 (38)	0	5 (63)	6 (75)	5 (63)	6 (75)	2 (29)	16 (76)	5 (56)	11 (92)
Volunteers (%) with ≥1 report of most frequent TEAEs across single-dose cohorts (≥2 reports receiving active treatment), *n* (%)													
Headache	1 (50)	0	19 (40)	2 (25)	0	4 (50)	4 (50)	4 (50)	5 (63)	1 (14)	7 (33)	2 (22)	5 (42)
Dizziness	0	0	6 (13)	0	0	2 (25)	0	2 (25)	2 (25)	0	0	0	0
Nausea	0	0	6 (13)	0	0	2 (25)	0	2 (25)	2 (25)	1 (14)	5 (24)	1 (11)	4 (33)
Tremor	0	0	0	0	0	0	0	0	0	1 (14)	4 (19)	0	4 (33)
Fatigue	0	0	0	0	0	0	0	0	0	0	2 (10)	0	2 (17)
Dyskinesia	0	0	0	0	0	0	0	0	0	0	2 (10)	0	2 (17)
Back/ extremity pain	0	3 (33)	3 (6)	0	0	0	1 (13)	1 (13)	1 (13)	0	0	0	0
Vomiting	0	0	2 (4)	0	0	1 (13)	0	1 (13)	0	0	0	0	0
Palpitations	0	0	2 (4)	0	0	1 (13)	1 (13)	0	0	0	0	0	0

from baseline or dose-related trends in pulmonary function testing or safety laboratory measures were observed. No dose-dependent changes were observed in physical or neurological examinations or the Movement Disorder Society-Unified Parkinson's Disease Rating Scale (MDS-UPDRS) Part III, Non-Motor Symptoms Scale, or Montreal Cognitive Assessment (MoCA) scores; such changes were not expected on the basis of the 28-day duration of dosing. Furthermore, by using these measures and the Columbia-Suicide Severity Rating Scale as safety outcomes, no evidence of clinically meaningful worsening of motor function, mood, or cognition occurred in patients treated with DNL201.

Treatment with DNL201 was not associated with changes in pulmonary (fig. S9, A to D) or renal function (fig. S10, A and B) across the phase 1 and 1b studies. No clinically meaningful changes from baseline or dose-related trends in diffusion capacity for carbon monoxide or forced vital capacity (fig. S9, A to D) were observed. Similarly, no clinically meaningful changes in renal function assessed by serum creatinine, blood urea nitrogen, or urine albumin were detected (fig. S10, A and B, and tables S11 and S12).

DISCUSSION

Pathogenic variants in *LRRK2* that increase its kinase activity greatly increase the risk for PD (*3*, *16*, *40*, *41*). Our data, consistent with other studies, demonstrate that LRRK2 activity is also increased in some patients with sporadic PD (*9*, *10*). LRRK2 has been shown to regulate many aspects of intracellular trafficking, and there is increasing evidence that lysosomal and autophagic defects play a key role in the pathogenic processes in PD (*6*, *7*). In our studies, DNL201 treatment has been shown to fully normalize lysosomal function in $LRRK2^{G2019S}$ primary mouse astrocytes and partially restore lysosomal proteolysis in *GBA*-variant cells, suggesting that LRRK2 inhibition may improve lysosomal function.

Here, we evaluated the LRRK2 inhibitor DNL201 in healthy volunteers and patients with PD in a phase 1 and phase 1b clinical trial, respectively. LRRK2 inhibition by DNL201 in preclinical models, as measured by phosphorylation of S935 in LRRK2, enabled dose projections for our clinical trials (Figs. 1 and 3). DNL201 modulated lysosomal endpoints in vitro and in vivo in rodents and nonhuman primates at clinically relevant doses, achieving about 80% inhibition of LRRK2 (Figs. 2 and 3). Our phase 1 and phase 1b clinical studies demonstrated dose-dependent inhibition of LRRK2 through measurement of pS935 LRRK2 and a downstream target of LRRK2, pT73 Rab10, in healthy volunteers and patients with PD, consistent with preclinical data. Evidence of lysosomal modulation, associated with a reduction in urinary BMP, was shown in both healthy volunteers and patients with PD at drug doses that were safe and generally well tolerated. Together, these results demonstrate that LRRK2 inhibition has potential as a disease-modifying treatment for PD supporting further investigation in long-term larger clinical trials in patients with PD.

Preclinical translational studies support the use of blood-based markers for projecting LRRK2 kinase inhibition in the brain of human volunteers. In nonhuman primates, the pharmacokinetics of DNL201 were comparable in plasma, CSF, and brain. In addition, pS935 LRRK2 inhibition was also similar in PBMCs and brain of nonhuman primates, suggesting that peripheral LRRK2 inhibition predicts inhibition in the CNS. In our phase 1 and phase 1b studies, DNL201 concentrations were similar in human CSF and plasma across a broad range of doses. Our data show that LRRK2 inhibition was quantitatively related to DNL201 concentrations in preclinical animal models, healthy volunteers, and patients with PD. Moreover, the pharmacokinetics are comparable in plasma, CSF, and brain in nonclinical studies, suggesting that peripheral pharmacodynamics are likely to indicate the extent of LRRK2 inhibition in the brain (Fig. 3, C and D). Development of clinically translatable CSF markers of LRRK2 inhibition and modulation of downstream pathways is being actively pursued to enable more direct measurement of LRRK2 inhibition in the CNS.

In our phase 1 and phase 1b studies, treatment with DNL201 demonstrated evidence of an impact on lysosomal function based on a dose-dependent reduction in urinary BMP concentration in both healthy volunteers and patients with PD. Urinary BMP has emerged as a potentially important marker of lysosomal function. Increased LRRK2 kinase activity and an increase in urinary BMP of about threefold are evident in *LRRK2* mutation carriers (*19*). Treatment with LRRK2 inhibitors reduced LRRK2 kinase activity and urinary BMP in animals (*20*). Our clinical trial results are consistent with this finding, demonstrating a reduction in urine BMP at DNL201 doses with high LRRK2 inhibition (>80%) in both healthy volunteers and patients with PD irrespective of *LRRK2* mutation, and suggesting that modulation of lysosomal function is independent of baseline BMP. The >80% inhibition of LRRK2 that was required to observe a reduction in BMP in urine may reflect a change in extracellular BMP resulting from cellular processes downstream of LRRK2 due to modulation of lysosomal function rather than being a direct biochemical target of LRRK2 activity. The relationship between urine BMP reduction and LRRK2 inhibition will need to be explored in more detail in future clinical studies.

The underlying mechanism for reduction in urinary BMP that occurs with LRRK2 inhibition remains unclear; however, changes in urinary BMP appear to correlate with alterations in lysosomal function, and BMP has been identified as a potential marker to measure the impact of LRRK2 inhibition on the lysosomal pathway (*20*, *27*). LRRK2 inhibition may reduce urinary BMP by modulating the extracellular transport of BMP-containing vesicles from endolysosomes through mechanisms potentially dependent on Rab phosphorylation, resulting in decreased BMP concentration in urine. Preclinical data reported here demonstrate that the reduction in urinary BMP that occurs with LRRK2 inhibition is accompanied by an increase in renal BMP, suggesting that LRRK2 inhibition may regulate urine BMP by reducing the extracellular release of BMP-containing vesicles from kidney tissue.

At drug doses that demonstrate LRRK2 inhibition, on-target effects in the lung (vacuolation of type II pneumocytes) were observed in early nonhuman primate studies evaluating LRRK2 inhibitors, delaying the advancement of LRRK2 inhibitors into the clinic (*20*). However, with thorough evaluation across multiple LRRK2 inhibitors at doses expected to demonstrate substantial kinase inhibition, these on-target changes were found to be nonadverse and reversible, with no measurable functional change (*22*). Previous studies described only nonclinical safety of small-molecule LRRK2 inhibitors in nonhuman primates for ≤28 days of repeat dosing, in which vacuolation in type II pneumocytes did not affect lung function tests or surfactant secretion end points (*20*, *22*). In the current study, long-term treatment with DNL201 in cynomolgus macaques for 39 weeks, a dosing duration demonstrated to identify late-occurring toxicities and progression of toxicities (*28*), showed sustained drug exposures and nonadverse microscopic findings in

the lung. Different doses of DNL201 that demonstrated kinase inhibition were associated with increased size and number of lamellar bodies (lysosome-related organelles) in type II pneumocytes in the macaque lung. These findings were consistent with previous reports (*20*, *22*), did not show progression over time compared with shorter studies, had no discernable functional effects, and were not associated with secondary degenerative or inflammatory effects (including evaluations by electron microscopy). These results were considered nonadverse and were reversible upon cessation of treatment. Therefore, these data indicate that DNL201 has a low risk of affecting respiratory function in humans at doses in the therapeutic range and support the use of LRRK2 inhibitors for chronic treatment of PD.

In the phase 1 and phase 1b studies reported here, DNL201 was generally well tolerated across a broad range of doses. These studies evaluated LRRK2 inhibition in both healthy volunteers and patients with PD, including DNL201 exposure, degree of LRRK2 inhibition, safety, and tolerability. There was an increased incidence of headaches in the DNL201-treated versus placebo-treated healthy volunteers and patients with PD. Whereas the potential mechanism for DNL201-related headaches is unclear, PDE5 inhibition is a consideration given that headaches have been known to occur in individuals taking PDE5 inhibitors (*42*). Lumbar punctures were used in both studies, which may have also contributed to the headaches.

PD patients with and without *LRRK2* mutations were included in the phase 1b study to obtain a preliminary assessment of potential pharmacokinetic, pharmacodynamic (pS935 LRRK2, pT73 Rab10, or BMP), and safety differences in *LRRK2* mutation carriers. The number of enrolled patients with *LRRK2* mutations was small, comprising about one-third of the phase 1b population. However, on the basis of this study, no genotype-associated differences were apparent in the outcomes. In addition, it was important to evaluate whether patients with PD were more susceptible to drug-induced AEs compared with healthy volunteers. Potential off-target, hemodynamic effects of PDE3 or PDE5 inhibition were prospectively monitored as blood pressure effects may differ in patients with PD because of disease-related autonomic dysfunction or concomitant use of dopaminergic medications. PDE5 inhibitor medications were excluded during the study; however, other vasodilators were allowed. Coadministration of an α-blocker with DNL201 was associated with orthostatic hypotension in one patient. There did not appear to be increased sensitivity of patients with PD to blood pressure changes during treatment with DNL201 compared to healthy volunteers; however, the potential for hemodynamic effects of DNL201 and specific drug-drug interactions warrants further study. The potential PDE3 and PDE5 inhibitory effects appeared to be off-target effects specific to DNL201 rather than LRRK2 inhibitors in general. Overall, the pharmacokinetic profile, extent of LRRK2 inhibition, and safety in patients with PD were similar to those in healthy volunteers.

In our human studies, no clinically meaningful changes in pulmonary or renal function were observed during a 28-day treatment period at drug doses demonstrating substantial LRRK2 inhibition and lysosomal pathway engagement. However, the possibility of unforeseen adverse events with sustained high LRRK2 inhibition in humans over months to years cannot be excluded. Therefore, future studies of LRRK2 inhibitors should evaluate safety over a longer treatment period at doses demonstrating near-maximal inhibition with evidence for modulation of lysosomal biomarkers. Support for the safety of long-term LRRK2 inhibition may be derived from two independent studies evaluating LRRK2 loss-of-function genetic variant carriers. Reduction in LRRK2 protein of about 50% in loss-of-function heterozygous carriers and possibly even up to 100% in one homozygous adult carrier appeared to demonstrate no impact on life expectancy and no increase in renal or pulmonary disease or other conditions (*43*, *44*). Overall, the safety data for DNL201 in nonclinical chronic toxicity studies and the phase 1 and phase 1b clinical trials provide an acceptable safety profile for continued clinical study.

Our phase 1 and phase 1b studies have several limitations. The small sample sizes, in particular for the *LRRK2* mutation carriers, limit the comparison of the outcomes in the *LRRK2* mutation carriers compared to patients with sporadic PD. The short duration of this study was not sufficient to study the clinical efficacy of DNL201, which would need to be evaluated in larger studies of longer duration. Determining the link between LRRK2-related marker changes (pS935 LRRK2, pT73 Rab10, and urinary BMP) and clinical improvement in PD also requires longer-term treatment coupled with efficacy evaluations. Therefore, additional clinical studies are needed to evaluate whether the reduction in LRRK2 activity and corresponding effects on lysosomal function due to treatment with LRRK2 inhibitors translate to a reduction in the progression of PD symptomatology.

Currently, no disease-modifying treatments for PD are available. Evidence suggests that increased LRRK2 activity is an important contributor to PD pathology through its effects on the lysosomal pathway (*11*). LRRK2 inhibitors represent a new class of investigational therapeutics with the potential to address a key aspect underlying the biology of PD, lysosomal dysfunction, and provide the possibility of reducing the rate of disease progression. Our nonclinical and human clinical data in healthy volunteers and in patients with PD have demonstrated the safety and tolerability of DNL201 at doses with substantial LRRK2 target and lysosomal pathway engagement. DNL201 provides proof of mechanism in humans and demonstrates characteristics of a viable therapeutic. On the basis of the totality of data to date for two chemically distinct LRRK2 inhibitors, DNL201 and BIIB122 (DNL151), both have met requirements to proceed into late-stage clinical studies. Selection of BIIB122 was made because of its pharmacokinetic properties that provide additional dosing regimen flexibility.

MATERIALS AND METHODS

Study design

This translational study involved evaluation of the underlying biology of LRRK2-dependent changes in lysosomal morphology in experiments using primary mouse astrocytes and human microglia. To evaluate DNL201 potency, inhibitory activity, and impact on the lysosomal pathway, experiments were conducted using cell models and animals (rodents and cynomolgus macaques). Preclinical toxicology assessments were completed in rodents and cynomolgus macaques. Clinical studies administering DNL201 in healthy volunteers (phase 1) and patients with PD (phase 1b) were conducted to evaluate the pharmacokinetics, amount of LRRK2 inhibition, modulation of lysosomal function, and safety in humans.

Analysis of LRRK2-dependent changes in lysosomal morphology

H4 cells {human neuroglioma cell line [American Type Culture Collection (ATCC) catalog no. HTB-148} were plated in 96-well plates (Cell Carrier Ultra plates, PerkinElmer, Waltham, MA) at a density of 5000 cells per well in Gibco Dulbecco's modified Eagle's

medium [DMEM, Thermo Fisher Scientific (TFS), Waltham, MA] and 10% fetal bovine serum (FBS). After 24 hours, lentiviruses encoding green fluorescent protein (GFP)–LRRK2 or GFP-LRRK2 G2019S (purchased from KU Leuven viral core, KU Leuven, Leuven, Belgium) were added to the H4 cells (final volume, 100 μl of medium per well, targeting multiplicity of infection of 3). About 18 hours later, medium was removed and exchanged for DMEM/10% FBS plus dimethyl sulfoxide (DMSO) (vehicle) or 0.3 μM DNL201. Two days later, fresh medium (with vehicle or DNL201) was added, and cells were incubated for an additional 24 hours (72 hours total treatment with vehicle or DNL201). Cells were fixed in 4% paraformaldehyde (PFA) in phosphate-buffered saline (PBS) and permeabilized with 0.01% Triton X-100 in 10% normal goat serum in PBS (blocking buffer). Cells were labeled using mouse anti-Lamp2 (H4B4, Abcam, Cambridge, UK) overnight at 4°C and followed by secondary detection using Alexa 568–conjugated goat anti-mouse, 4′,6-diamidino-2-phenylindole (DAPI), and HCS Cell Mask Deep Red (TFS). Cells were imaged using the Opera Phenix spinning-disk confocal microscope (PerkinElmer) (63× water objective; 405, 561, and 640 laser lines).

Imaging analysis was performed using Harmony software (PerkinElmer). Nuclei were identified using DAPI stain to identify individual cells, and the cytoplasmic area for each cell was identified using the HCS CellMask Deep Red signal. The spot analysis building block was used to identify individual lysosomes (using anti-LAMP2 signal). The percentage of cells with coalesced lysosomes, defined as ≥1 lysosome >3 μm in diameter, were divided by the total number of cells analyzed. These values were shown as a percentage of cells within separate experiments that contained any lysosomes with a diameter >3 μm.

Lysosomal protein turnover analysis in primary mouse astrocytes and Gaucher patient fibroblasts

To determine whether LRRK2^{G2019S} expression altered protein turnover and whether kinase activity improved lysosomal function, protein turnover via lysosomes was quantified using a modified, previously described, high-throughput, imaging-based assay (*43*). Primary mixed glial cultures from postnatal (P1 to P3) wild-type and *LRRK2*^{G2019S} KI mice (C57BL/6-Lrrk2tm4.1Arte; originally generated by the Michael J. Fox Foundation, New York, NY) maintained on a C57BL/6NTac genetic background were used for these studies (Taconic, model no 13940) (*44*). This model is a constitutive knockin of the human *G2019S* point mutation into exon 41 of the mouse *LRRK2* gene. To determine whether GBA variant cells had altered lysosomal protein turnover and whether LRRK2 kinase inhibition may modulate lysosomal proteolysis in these cells, Gaucher disease type 2 fibroblasts that were homozygous for the *L444P* variant and age-matched healthy control fibroblasts were obtained from Coriell Institute for Medical Research Biobank (catalog IDs: GM03349, GM05565, GM05659, GM08760, and GM00877).

Protein turnover was measured using L-azidohomoalanine (AHA) labeling to quantify long-lived protein degradation. AHA is used as a surrogate for L-methionine, and the AHA probe is incorporated into proteins during protein synthesis. After a short chase to remove short-lived proteins, the amount of long-lived AHA-containing proteins was visualized through a "click" reaction between the AHA probe and a fluorescently tagged alkyne probe. Briefly, mixed glial cells were plated into a 96-well plate at a density of 50,000 cells per well. Cells were treated with either vehicle or 2 μM (micromolar) DNL201 24 hours before AHA labeling and were maintained in the medium for the duration of the study. After 24 hours, the medium was replaced with methionine-free medium with or without AHA (negative control for staining). After 16 to 18 hours of labeling, the medium without AHA and containing a 10× excess of methionine was added for 2 hours. Cells were then incubated in DMEM +10% FBS with 10× methionine alone or supplemented with 50 nmol bafilomycin A (to assess the lysosomal component of long-lived degradation) for 24 hours. Cells were fixed with 4% PFA and permeabilized with 0.05% Triton X-100, and then the click reaction occurred between the azide group of AHA and an Alexa 488–conjugated alkyne probe (TFS) to label all AHA-containing proteins within cells. Cells were then labeled with DAPI and HCS CellMask Deep Red to visualize the nuclei and cytoplasm of each cell. Cells were imaged using the Opera Phenix spinning-disk confocal microscope (40× water objective; 405, 488, and 647 laser lines).

Imaging analysis was performed using Harmony software (PerkinElmer). Briefly, nuclei were identified using the DAPI stain to identify individual cells, and the cytoplasmic area for each cell was identified using the HCS CellMask Deep Red signal. AHA-containing proteins per cell were quantified by measuring the average intensity of the 488-modified AHA probe per cell.

Measurement of DNL201 potency in human PBMCs

LRRK2^{G2019S} carriers and noncarriers (with and without a self-reported PD diagnosis) were recruited from 2016 to 2017 {study IDs: SAN-BB-01 [approved by Quorum Review independent review board (IRB)], PLMDEN201609v1 (approved by New England IRB), and US-IRB-13-2016.1 (approved by E&I Review Services)}. PBMCs from two donors for pS935 LRRK2 and pT73 Rab10 dose-response comparison were obtained from AllCells (Alameda, CA).

Cryopreserved PBMC vials were rapidly thawed in a water bath. Cells were briefly washed twice and plated in PBMC medium [RPMI 1640 with GlutaMAX (TFS, Waltham, MA), 10% heat-inactivated FBS, and 1% penicillin-streptomycin] in a 96-well round-bottom plate at 3,000,000 cells per well (for pT73 Rab10/pS935 LRRK2 comparison) or 300,000 cells per well (for comparison of potency in LRRK2^{G2019S} carrier PBMCs). Dilutions of DNL201 were prepared by serial dilution of a 50 mM working stock of DNL201 in DMSO into PBMC medium. The PBMC/DNL201 mixture was incubated for 1 hour at 37°C. Cells were briefly resuspended, transferred to a 96-well round-bottom plate, briefly centrifuged, and then resuspended in ice-cold PBMC lysis buffer [1× cell lysis buffer (Cell Signaling Technology, Danvers, MA, catalog no. 9803) with PhosSTOP phosphatase inhibitor (Sigma-Aldrich, St. Louis, MO, 04906837001), complete protease inhibitor (Roche, Basel, Switzerland, 04693159001), and Benzonase (Sigma-Aldrich; E8263)]. Lysates were placed on ice for 20 min and then spun at maximum speed in a benchtop centrifuge for 20 min at 4°C. Supernatants were collected into new plates for pS935 LRRK2 and pT73 Rab10 immunoassay analysis in 96-well format as described below. DNL201 concentrations were adjusted for protein binding in 10% FBS (70% unbound). Data were fit to a four-parameter logistic curve in GraphPad Prism version 8 (GraphPad, San Diego, CA).

Measurement of DNL201's inhibition of LRRK2 in HEK293T cells

HEK293T cells (ATCC, CRL-11268) were seeded and incubated (see the Supplementary Materials and Methods for full description). Using the incubated HEK293T cells, 100 μl of the compound-containing medium was replaced with 100 μl of lysis buffer. The plates were sealed, shaken at 4°C for 30 min, and then stored at −20°C. On day 5,

the Flag antibody (monoclonal ANTI-FLAG, M2 antibody, Sigma-Aldrich, F3165) was diluted (2 μg/25 μl per well) in PBS [50 μl (3.9 μg/μl) of FLAG antibody +2.5 ml PBS], added into an MSD plate (MSD-L15XB-3), and incubated for 2 hours at room temperature. The plate was centrifuged at 1000 rpm for 10 s and shaken with multidrop for 10 s. The Flag antibody was then discarded and washed two times with 300 μl per well. Then, 50 μl per well of block buffer (LiCor, 927-40000) was added, and the plates were incubated for 2 hours at room temperature. The Flag antibody was again discarded and washed two times with 300 μl per well. The cell lysate (25 μl) was then transferred into a 96-well MSD plate and incubated for 1 hour at room temperature. The lysate was discarded and washed three times with 300 μl per well of wash buffer. The pS1292 antibody (Abcam, 203181) was diluted (1:100) with blocking buffer by adding 25 μl per well of antibody into a 96-well plate. In the case of pS935 antibody (Abcam, 133450), it was diluted (1:200). The antibody was then discarded and washed three times with 300 μl per well (96-well plate). The sulfotag goat anti-rabbit antibody (R32AB-1) was diluted (1:500) with blocking buffer by adding 25 μl per well of antibody into a 96-well plate and then incubated for 1 hour at room temperature. The antibody was then discarded and washed three times with 300 μl per well. A 2× reading buffer was prepared by a 1:1 dilution of 4× MSD reading buffer (MSD-R92TC-1) with MilliQ water. The wash buffer was then discarded by adding 150 μl per well of 2× reading buffer into each well. After a 3-min incubation, the MSD plates were read within 15 min.

Immunoassays

pS935 LRRK2 and pT73 Rab10 analyses were performed as previously described (*36*). Glyceraldehyde-3-phosphate dehydrogenase (GAPDH) analysis was performed according to the manufacturer's instructions (MSD catalog no. K151PWD).

Measurement of DNL201 potency in iMG

Human iMG were generated as previously described (*45*). Dose-response curves for both pS935 LRRK2 and pT73 Rab10 were generated in wild-type human iMG after treatment with varying concentrations of DNL201. Working dilutions of DNL201 were prepared by serial dilution of a 50 mM working stock of DNL201 in DMSO in C+++ medium, and wild-type iMG were incubated in the presence of DNL201 for 1 hour at 37°C. Cells were briefly washed in ice-cold PBS and then resuspended in ice-cold PBMC lysis buffer [1× cell lysis buffer (Cell Signaling Technology, Danvers, MA, catalog no. 9803) with PhosSTOP phosphatase inhibitor (Sigma-Aldrich, St. Louis, MO, 04906837001), complete protease inhibitor (Roche, Basel, Switzerland, 04693159001), and Benzonase (Sigma-Aldrich, E8263)]. Lysates were placed on ice for 20 min, transferred to a 96-well V-bottom plate (Falcon, no. 353263), and then spun at maximum speed in a benchtop centrifuge for 20 min at 4°C. Supernatants were collected into new plates for pS935 LRRK2 and pT73 Rab10 MSD-based analysis in a 96-well format as described above. DNL201 concentrations were adjusted for protein binding in 10% FBS. Data were fit to a four-parameter logistic curve in GraphPad Prism version 8 (GraphPad, San Diego, CA).

Nonclinical repeated dose toxicological assessments

The in-life phase (including clinical, ophthalmic, physical, respiratory, electrocardiogram, and neurological examinations), clinical pathology evaluation, necropsy, biospecimen collection, anatomic pathology evaluation, toxicokinetic assessment, and electron microscopy evaluation of the lungs were conducted at Covance Laboratories (Princeton, NJ). Histopathologic evaluation included a comprehensive tissue list and enhanced sampling and histopathology of the CNS. All scheduled necropsies were conducted about 24 hours after the last dose, and the expected C_{max} of the compounds was tested. Studies were conducted in 44 cynomolgus macaques (*Macaca fascicularis*) of Chinese origin, aged 26 to 36 months and weighing 1.9 to 2.7 kg at the start of the study (Covance, Princeton, NJ). The following doses were evaluated: 8, 16, and 32 mg/kg per day, as well as a vehicle control. Dose formulations were administered twice daily (BID) by oral gavage for 39 weeks at a dose volume of 5 ml/kg per dose (10 ml/kg per day). The second daily dose was administered 6 hours (+30 min) after the first daily dose.

Analysis of BMP concentrations in kidney and urine of wild-type and LRRK2^{G2019S} KI mice after LRRK2 inhibition

LRRK2^{G2019S} KI mice (C57BL/6-Lrrk2tm4.1Arte) were maintained on a C57BL/6NTac genetic background at Taconic Biosciences Inc. (Germantown, NY). Adult (7 to 9 months old) LRRK2^{G2019S} KI mice and their wild-type littermates were age-matched across treatment groups for experiments. MLi-2 (MedChemExpress, Monmouth Junction, NJ) was used as a tool LRRK2 inhibitor for in vivo experiments. Rodent chow with 10 kcal% fat and cornstarch was formulated into pellets containing MLi-2 (1000 ppm; 100 mg/kg diet) and irradiated for in-diet dosing (Research Diets Inc., New Brunswick, NJ; control diet D01060501i, MLi-2 diet D20040204i). Mice were provided vehicle or MLi-2 diet ad libitum for 7 days. Food weight and mouse body weight were monitored daily to evaluate diet consumption and animal health.

Urine was collected at baseline 1 day before the initiation of in-diet dosing and at terminal collection after 7 days of in-diet dosing. Urine samples were snap-frozen on dry ice and transferred to −80°C for storage. After 7 days of in-diet dosing, mice were euthanized for terminal collection of kidney samples. Mice were anesthetized with 2.5% tribromoethanol. Once deeply anesthetized, animals were transcardially perfused with ice-cold PBS using a peristaltic pump for a minimum of 3 min at a rate of 5 ml/min. After perfusion, the left kidney was removed and subdissected into the renal cortex and medulla. Each portion was weighed (20 ± 2 mg), collected in 1.5-ml Eppendorf tubes, frozen on dry ice, and stored at −80°C. Urine samples were prepared for BMP extraction, and extracted BMP species were quantified (see the Supplementary Materials for details).

Phase 1 study design

The phase 1, randomized, double-blind, placebo-controlled SAD and MAD oral dose study was conducted in healthy volunteers and elderly healthy volunteers (fig. S7, A and B). Primary objectives were to investigate the safety, tolerability, and plasma pharmacokinetics of single and multiple oral doses of DNL201. Secondary objectives included characterization of CSF DNL201 concentrations and whole-blood pS935 LRRK2 (pharmacodynamic marker). Exploratory marker measures were PBMC pT73 Rab10 and urine BMP (22:6/22:6).

The study was conducted at a single clinical research unit (CRU) in the United States and included SAD dosing cohorts (DNL201, 10 to 225 mg), MAD dosing cohorts (40 mg QD, 40 to 100 mg BID), and a MAD elderly healthy volunteer cohort (80 mg BID) (fig. S7, A and C). Eligible participants were randomized to receive DNL201

or placebo in a 3:1 ratio in SAD cohorts and in a 4:1 ratio in MAD cohorts. Eligible participants were male and female healthy volunteers aged 18 to 50 years (nonelderly cohorts) or 60 to 75 years (elderly cohorts), inclusive, with a body mass index between 18.5 and 31.0 kg/m^2 (nonelderly cohorts), or 18.5 and 35.0 kg/m^2 (elderly cohorts), inclusive, and a weight of ≥50.0 kg.

Phase 1b study design

The multicenter, randomized, double-blind, and placebo-controlled phase 1b clinical trial (NCT03710707) evaluated placebo, DNL201 30 mg, and DNL201 50 mg TID in patients with PD (fig. S7, C and D). The primary objective was to evaluate the safety and tolerability of DNL201 administered TID for 28 days. Secondary objectives were to characterize plasma DNL201 PK and CSF concentrations, whole-blood pS935 LRRK2, and PBMC pT73 Rab10. Exploratory marker measures were urine BMP (22:6/22:6) and CSF LRRK2.

The study was conducted at eight CRUs in the United States in two parts: Part 1 was a sentinel cohort (n = 4) randomized to placebo or DNL201 30 mg TID (1:3 ratio); part 2 included the remainder of patients (n = 24) randomized to placebo, DNL201 30 mg TID, or DNL201 50 mg TID (1:1:2 ratio) (fig. S7, B and D).

Eligible participants were men or women aged 30 to 80 years with a diagnosis of mild to moderate PD, Hoehn and Yahr scale 1 to 3, and the presence or absence of an *LRRK2* mutation. Patients with a MoCA score <24; clinically meaningful hepatic, pulmonary, or renal disorders; atypical forms of Parkinsonism; or neurological disorders other than PD were excluded.

Study outcomes

In both studies, safety and tolerability were assessed by AE monitoring, clinical laboratory tests (blood chemistries, hematology, and urinalysis), vital signs, electrocardiograms, physical and neurological examinations, and neurological assessments. For the multiple-dose cohorts only, the Columbia Suicide Severity Rating Scale and pulmonary function tests were assessed. Plasma and CSF pharmacokinetic parameters were evaluated. Pharmacodynamic assessments included percent change from baseline in whole-blood pS935 LRRK2, PBMC pT73 Rab10, and urine BMP (22:6/22:6). Average reduction from baseline in whole-blood pS935 LRRK2 and PBMC pT73 Rab10 over the dosing interval at steady state was calculated. Urine BMP (22:6/22:6) concentrations were reported as a ratio to urine creatinine concentrations [BMP (ng)/creatinine (mg)].

Statistics

Preclinical studies

Statistical comparison of the LRRK2 G2019S groups with and without DNL201 treatment in Fig. 2A was performed by an unpaired t test. Data in Fig. 2 (B and C) were normalized to the median value within each experiment and then to the wild-type (B) and control (C) vehicle-treated groups, respectively. Statistical significance was determined using two-way analysis of variance (ANOVA) with multiple comparison adjustments based on Dunnett's method. Relative abundance BMP values in fig. 3 (E to G) were log-transformed and analyzed using an analysis of covariance (ANCOVA) model with terms for treatment, genotype, and treatment by genotype interaction, with adjustment by sex, and for urine, by predose BMP concentrations. Statistical significance was assessed at nominal significance levels. For fig. S1 (A and B), IC_{50} values for the pS935 LRRK2 dose-response curves between groups were compared using a global F test of the best-fit four-parameter logistic curves, in GraphPad Prism version 8. In fig. S5, pairwise group comparisons were performed using a linear mixed-effects model on log-transformed values, accounting for repeat patient measurements among a subset of the samples, with adjustment by age and sex. Nominal P values were presented. All statistical tests were performed two-sided.

Clinical studies

Sample sizes were not based on power calculations but were considered sufficient to achieve the study objectives. For each study, data were summarized by treatment group (pooled placebo group and each DNL201 dose group). Demographic and other baseline characteristics, safety, pharmacokinetics, and pharmacodynamic data were summarized using descriptive statistics. The incidence of TEAEs was summarized for the safety population (treated participants). TEAEs were defined as AEs that occurred or worsened after initiation of study drug.

SUPPLEMENTARY MATERIALS

www.science.org/doi/10.1126/scitranslmed.abj2658
Materials and Methods
Figs. S1 to S10
Tables S1 to S12
Data file S1
MDAR Reproducibility Checklist

View/request a protocol for this paper from *Bio-protocol*.

REFERENCES AND NOTES

1. L. Hirsch, N. Jette, A. Frolkis, T. Steeves, T. Pringsheim, The incidence of Parkinson's disease: A systematic review and meta-analysis. *Neuroepidemiology* **46**, 292–300 (2016).
2. M. A. Hely, J. G. L. Morris, W. G. Reid, R. Trafficante, Sydney Multicenter Study of Parkinson's disease: Non-L-dopa-responsive problems dominate at 15 years. *Mov. Disord.* **20**, 190–199 (2005).
3. C. Ren, Y. Ding, S. Wei, L. Guan, C. Zhang, Y. Ji, F. Wang, S. Yin, P. Yin, G2019S variation in LRRK2: An ideal model for the study of Parkinson's disease? *Front. Hum. Neurosci.* **13**, 306 (2019).
4. D. Chang, M. A. Nalls, I. B. Hallgrímsdóttir, J. Hunkapiller, M. van der Brug, F. Cai; International Parkinson's Disease Genomics Consortium; 23andMe Research Team, G. A. Kerchner, G. Ayalon, B. Bingol, M. Sheng, D. Hinds, T. W. Behrens, A. B. Singleton, T. R. Bhangale, R. R. Graham, A meta-analysis of genome-wide association studies identifies 17 new Parkinson's disease risk loci. *Nat. Genet.* **49**, 1511–1516 (2017).
5. M. Steger, F. Diez, H. S. Dhekne, P. Lis, R. S. Nirujogi, O. Karayel, F. Tonelli, T. N. Martinez, E. Lorentzen, S. R. Pfeffer, D. R. Alessi, M. Mann, Systematic proteomic analysis of LRRK2-mediated Rab GTPase phosphorylation establishes a connection to ciliogenesis. *eLife* **6**, e31012 (2017).
6. L. Bonet-Ponce, M. R. Cookson, LRRK2 recruitment, activity, and function in organelles. *FEBS J.* 10.1111/febs.16099 (2021).
7. M. Madureira, N. Connor-Robson, R. Wade-Martins, LRRK2: Autophagy and lysosomal activity. *Front. Neurosci.* **14**, 498 (2020).
8. R. Mir, F. Tonelli, P. Lis, T. Macartney, N. K. Polinski, T. N. Martinez, M. Y. Chou, A. J. M. Howden, T. König, C. Hotzy, I. Milenkovic, T. Brücke, A. Zimprich, E. Sammler, D. R. Alessi, The Parkinson's disease VPS35[D620N] mutation enhances LRRK2-mediated Rab protein phosphorylation in mouse and human. *Biochem. J.* **475**, 1861–1883 (2018).
9. R. Di Maio, E. K. Hoffman, E. M. Rocha, M. T. Keeney, L. H. Sanders, B. R. De Miranda, A. Zharikov, A. Van Laar, A. F. Stepan, T. A. Lanz, J. K. Kofler, E. A. Burton, D. R. Alessi, T. G. Hastings, J. T. Greenamyre, LRRK2 activation in idiopathic Parkinson's disease. *Sci. Transl. Med.* **10**, eaar5429 (2018).
10. K. B. Fraser, A. B. Rawlins, R. G. Clark, R. N. Alcalay, D. G. Standaert, N. Liu, A. B. West; Parkinson's Disease Biomarker Program Consortium, Ser(P)-1292 LRRK2 in urinary exosomes is elevated in idiopathic Parkinson's disease. *Mov. Disord.* **31**, 1543–1550 (2016).
11. R. L. Wallings, S. W. Humble, M. E. Ward, R. Wade-Martins, Lysosomal dysfunction at the centre of Parkinson's disease and frontotemporal dementia/amyotrophic lateral sclerosis. *Trends Neurosci.* **42**, 899–912 (2019).
12. D. Ysselstein, M. Nguyen, T. J. Young, A. Severino, M. Schwake, K. Merchant, D. Krainc, LRRK2 kinase activity regulates lysosomal glucocerebrosidase in neurons derived from Parkinson's disease patients. *Nat. Commun.* **10**, 5570 (2019).

13. A. Sanyal, M. P. DeAndrade, H. S. Novis, S. Lin, J. Chang, N. Lengacher, J. J. Tomlinson, M. G. Tansey, M. J. LaVoie, Lysosome and inflammatory defects in GBA1-mutant astrocytes are normalized by LRRK2 inhibition. *Mov. Disord.* **35**, 760–773 (2020).
14. K. B. Fraser, M. S. Moehle, R. N. Alcalay, A. B. West; LRRK2 Cohort Consortium, Urinary LRRK2 phosphorylation predicts Parkinsonian phenotypes in G2019S LRRK2 carriers. *Neurology* **86**, 994–999 (2016).
15. S. Wang, K. Kelly, J. M. Brotchie, J. B. Koprich, A. B. West, Exosome markers of LRRK2 kinase inhibition. *NPJ Parkinsons Dis.* **6**, 32 (2020).
16. Z. Sheng, S. Zhang, D. Bustos, T. Kleinheinz, C. E. Le Pichon, S. L. Dominguez, H. O. Solanoy, J. Drummond, X. Zhang, X. Ding, F. Cai, Q. Song, X. Li, Z. Yue, M. P. van der Brug, D. J. Burdick, J. Gunzner-Toste, H. Chen, X. Liu, A. A. Estrada, Z. K. Sweeney, K. Scearce-Levie, J. G. Moffat, D. S. Kirkpatrick, H. Zhu, Ser1292 autophosphorylation is an indicator of LRRK2 kinase activity and contributes to the cellular effects of PD mutations. *Sci. Transl. Med.* **4**, 164ra161 (2012).
17. G. F. Grabner, N. Fawzy, R. Schreiber, L. M. Pusch, D. Bulfon, H. Koefeler, T. O. Eichmann, A. Lass, M. Schweiger, G. Marsche, G. Schoiswohl, U. Taschler, R. Zimmermann, Metabolic regulation of the lysosomal cofactor bis(monoacylglycero)phosphate in mice. *J. Lipid Res.* **61**, 995–1003 (2020).
18. P. J. Meikle, S. Duplock, D. Blacklock, P. D. Whitfield, G. Macintosh, J. J. Hopwood, M. Fuller, Effect of lysosomal storage on bis(monoacylglycero)phosphate. *Biochem. J.* **411**, 71–78 (2008).
19. R. N. Alcalay, F. Hsieh, E. Tengstrand, S. Padmanabhan, M. Baptista, C. Kehoe, S. Narayan, A. K. Boehme, K. Merchant, Higher urine bis(monoacylglycerol)phosphate levels in LRRK2 G2019S mutation carriers: Implications for therapeutic development. *Mov. Disord.* **35**, 134–141 (2020).
20. R. N. Fuji, M. Flagella, M. Baca, M. A. Baptista, J. Brodbeck, B. K. Chan, B. K. Fiske, L. Honigberg, A. M. Jubb, P. Katavolos, D. W. Lee, S. C. Lewin-Koh, T. Lin, X. Liu, S. Liu, J. P. Lyssikatos, J. O'Mahony, M. Reichelt, M. Roose-Girma, Z. Sheng, T. Sherer, A. Smith, M. Solon, Z. K. Sweeney, J. Tarrant, A. Urkowitz, S. Warming, M. Yaylaoglu, S. Zhang, H. Zhu, A. A. Estrada, R. J. Watts, Effect of selective LRRK2 kinase inhibition on nonhuman primate lung. *Sci. Transl. Med.* **7**, 273ra15 (2015).
21. A. A. Estrada, B. K. Chan, C. Baker-Glenn, A. Beresford, D. J. Burdick, M. Chambers, H. Chen, S. L. Dominguez, J. Dotson, J. Drummond, M. Flagella, R. Fuji, A. Gill, J. Halladay, S. F. Harris, T. P. Heffron, T. Kleinheinz, D. W. Lee, C. E. Le Pichon, X. Liu, J. P. Lyssikatos, A. D. Medhurst, J. G. Moffat, K. Nash, K. Scearce-Levie, Z. Sheng, D. G. Shore, S. Wong, S. Zhang, X. Zhang, H. Zhu, Z. K. Sweeney, Discovery of highly potent, selective, and brain-penetrant aminopyrazole leucine-rich repeat kinase 2 (LRRK2) small molecule inhibitors. *J. Med. Chem.* **57**, 921–936 (2014).
22. M. A. S. Baptista, K. Merchant, T. Barrett, S. Bhargava, D. K. Bryce, J. M. Ellis, A. A. Estrada, M. J. Fell, B. K. Fiske, R. N. Fuji, P. Galatsis, A. G. Henry, S. Hill, W. Hirst, C. Houle, M. E. Kennedy, X. Liu, M. L. Maddess, C. Markgraf, H. Mei, W. A. Meier, E. Needle, S. Ploch, C. Royer, K. Rudolph, A. K. Sharma, A. Stepan, S. Steyn, C. Trost, Z. Yin, H. Yu, X. Wang, T. B. Sherer, LRRK2 inhibitors induce reversible changes in nonhuman primate lungs without measurable pulmonary deficits. *Sci. Transl. Med.* **12**, eaav0820 (2020).
23. H. Chen, B. K. Chan, J. Drummond, A. A. Estrada, J. Gunzner-Toste, X. Liu, Y. Liu, J. Moffat, D. Shore, Z. K. Sweeney, T. Tran, S. Wang, G. Zhao, H. Zhu, D. J. Burdick, Discovery of selective LRRK2 inhibitors guided by computational analysis and molecular modeling. *J. Med. Chem.* **55**, 5536–5545 (2012).
24. A. G. Henry, S. Aghamohammadzadeh, H. Samaroo, Y. Chen, K. Mou, E. Needle, W. D. Hirst, Pathogenic LRRK2 mutations, through increased kinase activity, produce enlarged lysosomes with reduced degradative capacity and increase ATP13A2 expression. *Hum. Mol. Genet.* **24**, 6013–6028 (2015).
25. E. Sidransky, G. Lopez, The link between the GBA gene and Parkinsonism. *Lancet Neurol.* **11**, 986–998 (2012).
26. A. Sanyal, H. S. Novis, E. Gasser, S. Lin, M. J. LaVoie, LRRK2 kinase inhibition rescues deficits in lysosome function due to heterozygous *GBA1* expression in human iPSC-derived neurons. *Front. Neurosci.* **14**, 442 (2020).
27. A. M. Miranda, Z. M. Lasiecka, Y. Xu, J. Neufeld, S. Shahriar, S. Simoes, R. B. Chan, T. G. Oliveira, S. A. Small, G. Di Paolo, Neuronal lysosomal dysfunction releases exosomes harboring APP C-terminal fragments and unique lipid signatures. *Nat. Commun.* **9**, 291 (2018).
28. J. J. DeGeorge, L. L. Meyers, M. Takahashi, J. F. Contrera, The duration of non-rodent toxicity studies for pharmaceuticals. International Conference on Harmonication (ICH). *Toxicol. Sci.* **49**, 143–155 (1999).
29. D. Ness, Z. Ren, S. Gardai, D. Sharpnack, V. J. Johnson, R. J. Brennan, E. F. Brigham, A. J. Olaharski, Leucine-rich repeat kinase 2 (LRRK2)-deficient rats exhibit renal tubule injury and perturbations in metabolic and immunological homeostasis. *PLOS ONE* **8**, e66164 (2013).
30. M. A. S. Baptista, K. D. Dave, M. A. Frasier, T. B. Sherer, M. Greeley, M. J. Beck, J. S. Varsho, G. A. Parker, C. Moore, M. J. Churchill, C. K. Meshul, B. K. Fiske, Loss of leucine-rich repeat kinase 2 (LRRK2) in rats leads to progressive abnormal phenotypes in peripheral organs. *PLOS ONE* **8**, e80705 (2013).
31. S. Padmanabhan, T. A. Lanz, D. Gorman, M. Wolfe, A. Joyce, C. Cabrera, R. Lawrence-Henderson, N. Levers, N. Joshi, T. C. Ma, C. Liong, S. Narayan, R. N. Alcalay, S. J. Hutten, M. A. S. Baptista, K. Merchant, An assessment of LRRK2 serine 935 phosphorylation in human peripheral blood mononuclear cells in idiopathic Parkinson's disease and G2019S LRRK2 cohorts. *J. Parkinsons Dis.* **10**, 623–629 (2020).
32. F. Atashrazm, D. Hammond, G. Perera, M. F. Bolliger, E. Matar, G. M. Halliday, B. Schüle, S. J. G. Lewis, R. J. Nichols, N. Dzamko, LRRK2-mediated Rab10 phosphorylation in immune cells from Parkinson's disease patients. *Mov. Disord.* **34**, 406–415 (2019).
33. Y. Fan, R. Nirujogi, A. Garrido, J. Martínez, A. Bergareche-Yarza, E. Mondragón Rezola, A. Vinagre Aragón, I. Croitoru, A. Gorostidi Pagola, L. Paternain Markinez, R. Alcalay, R. Hickman, J. Duering, N. Pratuseviciute, S. Padmanabhana, F. Valldeoriola , M. José Martí, E. Tolosa, D. Alessi, E. Sammler, R1441G but not G201S mutation enhances LRRK2 mediated Rab10 phosphorylation in human peripheral blood neutrophils. *medRxiv* 01.28.21249614, (2021); https://doi.org/10.1101/2021.01.28.21249614.
34. Y. Fan, A. J. M. Howden, A. R. Sarhan, P. Lis, G. Ito, T. N. Martinez, K. Brockmann, T. Gasser, D. R. Alessi, E. M. Sammler, Interrogating Parkinson's disease LRRK2 kinase pathway activity by assessing Rab10 phosphorylation in human neutrophils. *Biochem. J.* **475**, 23–44 (2018).
35. Ö. Karayel, F. Tonelli, S. Virreira Winter, P. E. Geyer, Y. Fan, E. M. Sammler, D. R. Alessi, M. Steger, M. Mann, Accurate MS-based Rab10 phosphorylation stoichiometry determination as readout for LRRK2 activity in Parkinson's disease. *Mol. Cell. Proteomics* **19**, 1546–1560 (2020).
36. X. Wang, E. Negrou, M. T. Maloney, V. V. Bondar, S. V. Andrews, M. Montalban, C. Llapashtica, R. Maciuca, H. Nguyen, H. Solanoy, A. Arguello, L. Przybyla, N. J. Moerke, S. Huntwork-Rodriguez, A. G. Henry, Understanding LRRK2 kinase activity in preclinical models and human subjects through quantitative analysis of LRRK2 and pT73 Rab10. *Sci. Rep.* **11**, 12900 (2021).
37. P. Lis, S. Burel, M. Steger, M. Mann, F. Brown, F. Diez, F. Tonelli, J. L. Holton, P. W. Ho, S. L. Ho, M. Y. Chou, N. K. Polinski, T. N. Martinez, P. Davies, D. R. Alessi, Development of phospho-specific Rab protein antibodies to monitor in vivo activity of the LRRK2 Parkinson's disease kinase. *Biochem. J.* **475**, 1–22 (2018).
38. K. Melachroinou, M. S. Kang, C. Liong, S. Narayan, N. Levers, N. Joshi, K. Kopil, S. J. Hutten, M. A. S. Baptista, S. Padmanabhan, U. J. Kang, L. Stefanis, R. N. Alcalay, H. J. Rideout, Elevated in vitro kinase activity in peripheral blood mononuclear cells of leucine-rich repeat kinase 2 G2019S carriers: A novel enzyme-linked immunosorbent assay-based method. *Mov. Disord.* **35**, 2095–2100 (2020).
39. M. L. Chen, R. M. Wu, LRRK 2 gene mutations in the pathophysiology of the ROCO domain and therapeutic targets for Parkinson's disease: A review. *J. Biomed. Sci.* **25**, 52 (2018).
40. A. B. West, D. J. Moore, C. Choi, S. A. Andrabi, X. Li, D. Dikeman, S. Biskup, Z. Zhang, K. L. Lim, V. L. Dawson, T. M. Dawson, Parkinson's disease-associated mutations in LRRK2 link enhanced GTP-binding and kinase activities to neuronal toxicity. *Hum. Mol. Genet.* **16**, 223–232 (2007).
41. N. L. Khan, S. Jain, J. M. Lynch, N. Pavese, P. Abou-Sleiman, J. L. Holton, D. G. Healy, W. P. Gilks, M. G. Sweeney, M. Ganguly, V. Gibbons, S. Gandhi, J. Vaughan, L. H. Eunson, R. Katzenschlager, J. Gayton, G. Lennox, T. Revesz, D. Nicholl, K. P. Bhatia, N. Quinn, D. Brooks, A. J. Lees, M. B. Davis, P. Piccini, A. B. Singleton, N. W. Wood, Mutations in the gene LRRK2 encoding dardarin (PARK8) cause familial Parkinson's disease: Clinical, pathological, olfactory and functional imaging and genetic data. *Brain* **128**, 2786–2796 (2005).
42. A. Rashid, The efficacy and safety of PDE5 inhibitors. *Clin. Cornerstone* **7**, 47–56 (2005).
43. N. Whiffin, I. M. Armean, A. Kleinman, J. L. Marshall, E. V. Minikel, J. K. Goodrich, N. M. Quaife, J. B. Cole, Q. Wang, K. J. Karczewski, B. B. Cummings, L. Francioli, K. Laricchia, A. Guan, B. Alipanahi, P. Morrison, M. A. S. Baptista, K. M. Merchant; Genome Aggregation Database Production Team; Genome Aggregation Database Consortium, J. S. Ware, A. S. Havulinna, B. Iliadou, J. J. Lee, G. N. Nadkarni, C. Whiteman, M. Daly, T. Esko, C. Hultman, R. J. F. Loos, L. Milani, A. Palotie, C. Pato, M. Pato, D. Saleheen, P. F. Sullivan, J. Alföldi, P. Cannon, D. G. MacArthur, The effect of LRRK2 loss-of-function variants in humans. *Nat. Med.* **26**, 869–877 (2020).
44. C. Beetz, A. Westenberger, R. Al-Ali, N. Ameziane, N. Alhashmi, R. M. Boustany, F. Al Mutairi, M. Alfadhel, Z. Al-Hassnan, M. AlSayed, K. K. Kandaswamy, O. Paknia, V. Skrahina, A. Rolfs, P. Bauer, LRRK2 loss-of-function variants in patients with rare diseases: No evidence for a phenotypic impact. *Mov. Disord.* **36**, 1029–1031 (2021).
45. B. J. Andreone, L. Przybyla, C. Llapashtica, A. Rana, S. S. Davis, B. van Lengerich, K. Lin, J. Shi, Y. Mei, G. Astarita, G. Di Paolo, T. Sandmann, K. M. Monroe, J. W. Lewcock, Alzheimer's-associated PLCγ2 is a signaling node required for both TREM2 function and the inflammatory response in human microglia. *Nat Neurosci* **23**, 927–938 (2020).

Acknowledgments: We thank the volunteers, patients, and their families who participated in the clinical studies. We thank M. Montalban for sample analysis. **Funding:** The research in this study was funded by Denali Therapeutics Inc. Support for third-party writing assistance, furnished by C. Gould of Health Interactions Inc., was provided by Denali Therapeutics Inc.

Author contributions: D.J. and M.D.T. were responsible for the development of the clinical study designs, execution of the phase 1 and phase 1b studies, and interpretation and analysis of the reported results. S.H.-R. and K.S.-L. participated in the study designs and interpretation of the reported results. A.G.H. participated in the study design, execution of preclinical studies, and interpretation of the reported results. J.C.S., R.D.M., and D.D. participated in the study design, execution, and interpretation of the preclinical safety studies. H.S. participated in the preclinical study designs, execution of preclinical studies, and interpreted and reported preclinical results. X.W., V.V.B., R.G., M.T.M., S.T.M., and A.A. participated in the execution of the preclinical studies and interpretation of the reported results. E.N. participated in preclinical and clinical data acquisition and interpretation of reported preclinical and clinical results. N.E.P. participated in the execution of preclinical studies. Y.Z. and R.D.M. participated in the study design, interpretation of the reported results, and design and execution of statistical analyses. L.H. participated in the execution of statistical analyses. A.K. participated in the study design and execution of the phase 1 and phase 1b studies. P.L. participated in the phase 1b study design, clinical assessments and data collection, and interpretation of results for the clinical studies. T.A.K. participated in clinical assessments, data acquisition, and interpretation of results for the phase 1 clinical study. D.K., A.E., I.G., A.S., J.A., and O.O. participated as site investigators for the phase 1b study completing clinical assessments, data acquisition, and interpretation of results for the clinical studies. S.S.D. participated in data acquisition of preclinical studies and reviewed and critiqued the manuscript. A.A.E., J.d.V., and Z.K.S. participated in the discovery and development of the compound DNL201. G.A. participated in the reporting and interpretation of clinical results. M.T.B. participated in the analysis and interpretation of the clinical pharmacokinetics data. B.K.W. and H.W. participated in the analysis and interpretation of pharmacokinetics data. H.N. participated in the preclinical study designs and execution of preclinical studies. C.H. participated in the development of the clinical study designs, provided oversight for execution of the phase 1 and phase 1b studies, and participated in the interpretation and analysis of the reported results. D.J., M.D.T., S.H.-R., K.S.-L., and M.T.B. drafted the paper, and all authors reviewed the paper. **Competing interests:** P.L. has served as a consultant or advisor for Acorda Therapeutics, Amneal, Appello, Axovant Biosciences, Biogen, Bukwang, Cavion, Denali Therapeutics Inc., F. Hoffmann–La Roche, Impel Neuropharma, Intec, Ipsen, Kyowa Kirin Hakko, Lundbeck, Merck, Merz, Mitsubishi Tanabe–NeuroDerm Neuropharma, Neurocrine, Noven, Parkinson's Study Group, Prexton Therapeutics, Revance Therapeutics, Saccadous, Supernus, and U.S. WorldMeds and has received speaker honoraria from Acorda Therapeutics, the American Academy of Neurology, the International Parkinson's's Disease and Movement Disorders Society, Neurocrine, Pallidan Labs, U.S. WorldMeds, and the World Parkinson's Congress. D.K. has served as an advisor for Colorado Clinical and Translational Sciences Institute (CCTSI) Data Safety Monitoring Board, Medtronic, Boston Scientific, Denali Therapeutics Inc., and AbbVie Pharmaceutics; D.K. has received honoraria from AbbVie Pharmaceutics and Boston Scientific and received grants from the National Institutes of Health and Boston Scientific. J.A. has served as a consultant or advisor to Abbott, AbbVie, Allergan, Boston Scientific, and Amneal and has received speaker honoraria from AbbVie, Allergan, Acorda, Boston Scientific, Impax, Teva Neuroscience, Neurocrine, Biogen, Sunovion, and Kyowa Kirin. J.A. has also received research support from Abbott, AbbVie, Revance, Neurocrine, Biogen, Boston Scientific, Centogene, Denali Therapeutics Inc., Sun Pharma, EIP Pharma, Sunovion, Theravance, Accorda, Amneal, and F. Hoffmann–La Roche. M.T.B., H.W., B.K.W., and Z.K.S. are consultants for Denali Therapeutics Inc. A.E. has consulted for or received speaker honoraria from Acadia, Affiris, Revenance and XW Laboratories Inc., Acorda, Adamas, Allergan, Biohaven, Ipsen, U.S. World Meds, Arbor, and Teva. A.S. has consulted for Biogen, Wave Life Sciences, Prevail, Bial Biotech, and Takeda and has received grant funding from the Michael J. Fox Foundation. A.E. is coinventor on U.S. patent no. 8,815,882 entitled "Pyraxole aminopyrimidine derivatives as LRRK2 modulators". S.H.-R., A.G.H., M.T.M., and X.W. are coinventors on U.S. patent no. 2021/0147573 entitled "Phospho-Rab antibodies, assays and methods of use thereof." **Data and materials availability:** All data associated with this study are present in the paper or the Supplementary Materials. DNL201 can be made available through a material transfer agreement by submitting a request at https://denalitherapeutics.com/contact.

Submitted 7 May 2021
Resubmitted 1 November 2021
Accepted 14 April 2022
Published 8 June 2022
10.1126/scitranslmed.abj2658

Science Translational Medicine

Preclinical and clinical evaluation of the LRRK2 inhibitor DNL201 for Parkinson's disease

Danna JenningsSarah Huntwork-RodriguezAnastasia G. HenryJennifer C. SasakiRené MeisnerDolores DiazHilda SolanoyXiang WangElvira NegrouVitaliy V. BondarRajarshi GhoshMichael T. MaloneyNicholas E. PropsonYuda ZhuRomeo D. MaciucaLaura HarrisAngela KayPeter LeWittT. Alex KingDrew KernAaron EllenbogenIra GoodmanAndrew SiderowfJason AldredOmid OmidvarShababa T. MasoudSonnet S. DavisAnnie ArguelloAnthony A. EstradaJavier de VicenteZachary K. SweeneyGiuseppe AstaritaMarie T. BorinBradley K. WongHarvey WongHoang NguyenKimberly Scearce-LevieCarole HoMatthew D. Troyer

Sci. Transl. Med., 14 (648), eabj2658. • DOI: 10.1126/scitranslmed.abj2658

A big step forward for Parkinson's disease

Inhibition of LRRK2 has emerged as a promising disease-modifying therapeutic target for Parkinson's disease. Jennings *et al.* now report evidence that DNL201, a first-in-class CNS-penetrant LRRK2 kinase inhibitor, reduces LRRK2 activity and restores lysosomal function in cellular and animal models. In healthy volunteers and patients with Parkinson's disease, DNL201 inhibited LRRK2 kinase activity and demonstrated an impact on lysosomal function at doses that were safe and generally well tolerated. As discussed in a related Focus, these findings provide support for advancing the investigation of LRRK2 inhibitors to late-stage clinical studies in patients with Parkinson's disease.

Science Translational Medicine (ISSN) is published by the American Association for the Advancement of Science. 1200 New York Avenue NW, Washington, DC 20005. The title *Science Translational Medicine* is a registered trademark of AAAS.